Heat transfer analysis of MHD carbon nanotubes flow over a stretching sheet

S.R.R. Reddy [1], *P. Bala Anki Reddy* [1,*], *Ali J. Chamkha* [2]

[*] *Email: pbarmaths@gmail.com*

[1] *Department of Mathematics, S.A.S., Vellore Institute of Technology, Vellore-632014, India.*

[2] *Mechanical Engineering Department, Prince Sultan Endowment for Energy and Environment, Prince Mohammad Bin Fahd University, Al- Khobar 31952, Saudi Arabia.*

Abstract: This article is intended for investigating the effect of aligned magnetic field flow and heat transfer of carbon nanotubes over a moving extensible stretching surface through a porous medium. Definitions of thermal radiation and heat generation/absorption are utilized in the thermal expression. Carbon nanotubes (SWCNTs and MWCNTs) and base fluids (seawater, blood and ethylene glycol) are used to explore the impacts of heat transfer characteristics. A similarity transformation is used to transform the governing boundary layer coupled partial differential equations into a system of non-linear ordinary differential equations, which are explored numerically using the Runge-Kutta fourth order method along with shooting

procedure. The stream lines are closer to the surface wall when lower values of magnetic parameter and porosity parameter. Strengthening the thermal radiation parameter value enhances the rate of heat transfer. A comparative study between the formerly published results and the present results for a special case is found to be in a tremendous agreement.

Keywords: Porous medium, aligned magnetic field, thermal radiation, heat generation/absorption, carbon nanotubes and slip model.

1 Introduction

During the last few years, the problems on heat transfer over a stretching sheet have attracted considerable interest because of its abundant industrialized and engineering applications such as the extrusion of sheet, hot rolling, shrinking wrapping, in the production of canvas materials over an extrusion process, the sweptback extrusion of soft sheer crystal and bundle wrapping. Zeeshan et al. (2016) studied the effect of ferromagnetic dipole and thermal radiation on the flow of viscous fluid past over a stretching sheet. The effects of thermal radiation, thermophoresis, Brownian motion, variable viscosity and magnetic field on an electrically conducting nanofluid over a radially stretching surface was presented by Makinde et al. (2016).

Bhatti et al. (2016) examined the entropy generation on MHD Powell-Eyring nanofluid through a permeable stretching surface. Mixed convection flow of thermal and solutal stratification on hydromagnetic nanofluid over an exponentially stretching surface with viscous dissipation effect has been analyzed by Besthapu et al. (2017). The effects of thermal radiation (Lu et al. (2018); Mohammdien et al. (2018); Reddy et al. (2018)), elastic deformation on nano-second grade (Kalaivanan et al. (2018)), chemical reaction (Bala Anki Reddy (2016); Hayat et al. (2017); Muthucumaraswamy (2002); Srinivas et al. (2014)), hydromagnetic (Bhatti and Rashidi (2017); Kandasamy et al. (2019); Turkyilmazoglu (2018a,b)) over a stretching sheet under different flow conditions have been reported. Ur Rehman et al. (2018) investigated the MHD stagnation-point flow of water-based nano-material influenced by a 3D exponential stretching surface.

There are different conditions in which the no-slip condition prompts wrong results, particularly when one is pondering non-Newtonian fluid or Nanofluid. For such liquids, the development is still represented by first principles, anyway, there are various circumstances where there may be a partial slip between the liquid and the boundary. In this circumstance, the standard no-slip condition at the boundary is replaced by the slip condi-

tion. The fluid flow in numerous applications in micro/nano organizations, for example, hard disk drive, micro-valve, micro-pumps and micro-beak are characterized by slip flow at the wall. Singh and Chamkha (2013) explored the dual solution for second-order slip flow and heat transfer on a linearly shrinking isothermal sheet. The effects of hydromagnetic, thermal radiation and second order slip flow of nanofluid over a stretching/shrinking sheet were discussed by Hakeem et al. (2015). Hayat et al. (2015) addressed the steady 3D hydromagnetic flow of nanofluid subjected to second order slip velocity and heterogeneous- homogeneous reactions. Melting heat transfer on second-order slip, viscous dissipation, and hydromagnetic convective flow of a nanofluid over an extending sheet was found by Mabood and Mastroberardino Mabood and Mastroberardino (2015).

The present days, nanotechnology is gaining more importance due to the applications in many industrial applications (electronics cooling, vehicle cooling, transformer cooling), transportation, nuclear reactors (nuclear power plants), engineering, medical sciences (cancer therapy and safer surgery by cooling and process industries). Chamkha et al. (2018) explored the partial slip effects on entropy generation and hydromagnetic combined convection in a lid-driven porous enclosure filled with a Cu – water nanofluid.More

recently, heat transfer on time-dependent hybrid nanofluid flow past (suspending Al2O3 and Cu in pure water) a stretching/shrinking sheet model was proposed by Waini et al. (2019). Aly (2019) introduced a direct and effective approach to analytically obtain the exact solution of graphenewater nanofluid flow over stretching/ shrinking sheet with suction/injection and heat source/sink.There have been many efforts to use carbon nanotubes in different situations and geometries. Some of the latest can be found in (Aly and Sayed (2017); Buongiorno (2006); Mustafa et al. (2018); Reddy and Bala Anki Reddy (2018)).

Carbon nanotubes are allotropes of carbon which are constructed in cylindrical tubes with nanometer scale in diameter and several millimeters in length. CNTs are able to conjugate or adsorb with a wide variety of therapeutic molecules (antibodies, drugs, enzymes, proteins, DNA, etc.). These nanoparticles directly penetrate into the cells and without metabolism during transportation in the body for drug delivery by keeping drugs proved to be a marvelous vehicle. CNTs are able to cross the blood-brain barrier by various targeting mechanisms for acting as effective delivery carriers for the target brain. Applications of Carbon Nanotubes in pharmacy and medicine are include drug, biomolecule, gene delivery to cells or organs, tissue regener-

ation, biosensor diagnostics and analysis, drug carriers to treat tumors, cancer therapy, antitumor immunotherapy, infection therapy, tissue regeneration and artificial implants neurodegenerative diseases and Alzheimer syndrome (Gaffney et al. (2014); He et al. (2013)).

Carbon nanotubes membranes used for reverse osmosis process in water purification (Ihsanullah (2019); Zhang et al. (2011)). CNTs have also been used as adsorbents to remove metal ions, fluoride, 1,2-dichlorobenzene, trihalomethanes and organic pollutants from the water. NaCl removal in salt-water solution using carbon nanotubes / activated carbon mixed electrodes (Tofighy and Mohammadi (2010); Zhang et al. (2006)). The hydromantic flow of SWCNTs and MWCNTs suspended in a salt water solution through a vertical cone with semi-angle was investigated by Ellahi et al. (2015). Kandasamy et al. (2016) observed the effect of SWCNTs on hydromantic unsteady flow with variable stream conditions over a porous wedge. Moreover, carbon nanotubes with conventional fluids used for heat transfer applications in automobiles restrict the performance and compactness of heat exchangers. Akbara et al. (2018) gave the numerical solution of Christov- Cattaneo heat flux model in CNTs over a porous extending surface with suction and injection. Three-dimensional rotating flow of hydromantic SWCNTs over a

stretching sheet in the presence of thermal radiation was developed by Nasir et al. (2018).

The use of thermal radiation is an essential in space technology, for example, space craft reentry aerodynamics, comical flight aeromechanics rockets, propulsion systems and plasma physics, and also in industrials applications, such as glass production and heater outline which works at high temperatures. A portion of the research workers (Khalid et al. (2018); Reddy and Reddy (2011); Reddy et al. (2012); Sheikholeslami and Rokni (2018); Turkyilmazoglu (2019)) were researched the thermal radiation over a stretching sheet/surface.

To the author's awareness, no exploration has been accounted for on impact of the aligned magnetic field on steady 2D flow over a moving extensible surface with velocity slip and Carbon Nanotubes. The main objective of the present paper works to analyze the influences of the aligned magnetic field on the boundary layer flow of a Casson fluid over an extending sheet in the presence of carbon nanotubes with velocity slip effect. The governing partial differential equations are converted into ordinary differential equations by a similarity transformation, and after that, they are solved numerically by using bvp4c with MATLAB software. The numerical values are obtained for

the skin friction coefficient and local Nusselt number as well as the velocity and temperature profiles.

2 Mathematical formulation

We examine the two-dimensional(x, y), steady, laminar, hydromagnetic fluid flow over a stretching sheet. The physical significance of nanofluid flow is organized in Fig. 1 . In a coordinate system, x and y are the surface of the geometry and vertical to the sheet respectively. The stretching velocity of the sheet is $u_s(x)$. The temperature distribution is $T_W(x)$, which is higher than the ambient temperature T_∞. A uniform magnetic field of strength B_0 is implemented in r direction. Here induced magnetic field is neglected due to small magnetic Reynolds number. The thermophysical properties of the nanofluids are given in Table 1. The governing equations of the continuity, momentum and energy are given by (see Aly and Sayed (2017); Liao (2004))

$$\frac{\partial u}{\partial x} + \frac{\partial v}{\partial y} = 0 \tag{1}$$

$$u\frac{\partial u}{\partial x} + v\frac{\partial u}{\partial y} = \nu_{nf}\frac{\partial^2 u}{\partial y^2} - \frac{\sigma B^2(x)}{\rho_{nf}}\sin^2\xi\ u - \frac{\nu_{nf}}{k_1}u \tag{2}$$

$$u\frac{\partial T}{\partial x} + v\frac{\partial T}{\partial y} = \frac{k_{nf}}{(\rho C_p)_{nf}}\frac{\partial^2 T}{\partial y^2} - \frac{1}{(\rho C_p)_{nf}}\frac{\partial q_r}{\partial y} + \frac{Q_0}{(\rho C_p)_{nf}}(T - T_\infty) \tag{3}$$

With the boundary conditions

$$\left.\begin{array}{l} u = u_s(x) + U_{slip}, v = 0,\ T = T_w(x)\ \ at\ y = 0, \\ u = 0,\ \ T \to T_\infty as\ \ y \to \infty, \\ u \to 0,\ T \to T_\infty\, as\ \ x \to -\infty \end{array}\right\} \tag{4}$$

Where ρ_{nf} is the effective density of the nanofluid, ν_{nf} is the kinematic viscosity of nanofluid and σ is the electrical conduction, $B(x)$ is the magnetic field, k_1 is the permeability parameter, Q_0 is the heat generation ($Q_0 > 0$) or absorption ($Q_0 < 0$) coefficient. These nanofluid quantities are defined as

$$\left.\begin{array}{l} \mu_{nf} = \frac{\mu_f}{(1-\phi)^{2.5}}, v_{nf} = \frac{\mu_{nf}}{\rho_{nf}}, \rho_{nf} = (1-\phi)\,\rho_f + \phi\rho_{CNT}, \\ (\rho C_p)_{nf} = (1-\phi)\,(\rho C_p)_f + \phi\,(\rho C_p)_{CNT}\,, \\ \alpha_{nf} = \frac{k_{nf}}{(\rho C_p)_{nf}}, \frac{k_{nf}}{k_f} = \frac{(1-\phi)+2\phi\frac{k_{CNT}}{k_{CNT}-k_f}\ln\frac{k_{CNT}+k_f}{2k_f}}{(1-\phi)+2\phi\frac{k_f}{k_{CNT}-k_f}\ln\frac{k_{CNT}+k_f}{2k_f}} \end{array}\right\} \tag{5}$$

The radiative heat flux q_r is given by

$$q_r = -\frac{4\sigma*}{3k*}\,\frac{\partial T^4}{\partial y} \tag{6}$$

If the temperature differences within the mass of fluid flow are sufficiently small, then Eq. (6) can be linearized by expanding T^4 into the Taylor's series about T_∞, we get

$$T^4 \cong 4T_\infty^3 T - 3T_\infty^4 \tag{7}$$

Therefore Eq. (3) becomes

$$u\frac{\partial T}{\partial x}+v\frac{\partial T}{\partial y}=\frac{k_{nf}}{(\rho C_p)_{nf}}\frac{\partial^2 T}{\partial y^2}-\frac{16\sigma^* T_\infty^3}{3k^*(\rho C_p)_{nf}}\frac{\partial^2 T}{\partial y^2}+\frac{Q_0}{(\rho C_p)_{nf}}(T-T_\infty) \quad (8)$$

$u_s(x)$ is consider of the form (see Kuiken (1981); Liao (2004))

$$u_s(x)=\left(\frac{x_0}{|x|}\right)^n U_0,\ n>0. \quad (9)$$

U_{slip} is consider in the form (see Singh and Chamkha (2013))

$$\left.\begin{aligned} U_{slip} &= \tfrac{2}{3}\left(\tfrac{3-\alpha_m l^3}{\alpha_m}-\tfrac{3}{2}\tfrac{1-l^2}{K_n}\right)\lambda_m\tfrac{\partial u}{\partial y}-\tfrac{1}{4}\left[l^4+\tfrac{2}{K_n^2}(1-l^2)\right]\lambda_m^2\tfrac{\partial^2 u}{\partial y^2} \\ &= A^*\tfrac{\partial u}{\partial y}+C^*\tfrac{\partial^2 u}{\partial y^2} \end{aligned}\right\} \quad (10)$$

Where $l=\min\left(\frac{1}{K_n},1\right)$, K_n is the Knudsen number, λ_m is the molecular mean free path, α_m is the momentum accommodation coefficient with $0\le\alpha_m\le 1$. Based on the definition of l, it is noticed that for any given value of K_n, we have $0\le l\le 1$. The mean free path of molecular is always +ve it results that C^* is a -ve number.

we introduce the self-similarity variables in the following form are given by

$$\left.\begin{aligned} &\eta=y\left(\tfrac{u_s}{2v_f|x|}\right)^{\frac{1}{2}},\quad f(\eta)=\tfrac{\psi}{\left(2v_f u_s|x|\right)^{\frac{1}{2}}},\ \theta(\eta)=\tfrac{T-T_\infty}{T_w-T_\infty}, \\ &T_w(x)=T_\infty+T_0\left(\tfrac{x_0}{|x|}\right)^m, B(x)=B_0\left(\tfrac{x_0}{|x|}\right)^{\frac{(n+1)}{2}}, \\ &k_1=k_0\left(\tfrac{x_0}{|x|}\right)^{-(n+1)} \end{aligned}\right\} \quad (11)$$

Where η is the similarity variable, $f(\eta)$ is the dimensionless stream function, $\theta(\eta)$ is the dimensionless temperature. ψ is the stream function which is defined by $u = \frac{\partial \psi}{\partial y}$ and $v = -\frac{\partial \psi}{\partial x}$. The above expression also satisfies the continuity Eq.(1). By using Eq. (11), the Eq. (2) and (8) reduced to:

$$\begin{aligned} \tfrac{1}{(1-\phi)^{2.5}} f''' - \left(1 - \phi + \phi \tfrac{\rho_{CNT}}{\rho_f}\right) \left[2nf'^2 - (n-1) f f''\right] \\ -2M \sin^2 \xi \; f' - \tfrac{2K}{(1-\phi)^{2.5}} f' = 0, \end{aligned} \tag{12}$$

$$\begin{aligned} \left(\tfrac{k_{nf}}{k_f} + \tfrac{4}{3}R\right) \theta'' + \Pr Q\theta \; - \Pr \left((1-\phi) + \phi \tfrac{(\rho C_p)_{CNT}}{(\rho C_p)_f}\right) \\ (2mf'\theta - (n-1) f\theta') = 0, \end{aligned} \tag{13}$$

The transformed boundary conditions are:

$$\left.\begin{array}{ll} f(0) = 0, \; f'(0) - 1 = \delta f'''(0) + \lambda f''(0), \, \theta(0) = 1 & \text{at } \eta \to 0 \\ f'(\eta) \to 0, \; \theta(\eta) \to 0 & \text{as } \eta \to \infty \end{array}\right\} \tag{14}$$

Where λ, δ, M, K, Pr, R and Q are the first order velocity slip, second-order velocity slip, magnetic parameter, porosity parameter, Prandtl number, radiation parameter and heat generation/absorption ($Q > 0$ heat generation $Q < 0$ heat absorption) parameter respectively.

$$M = \tfrac{\sigma_f B_0^2 x_0}{\rho_f U_0}, \; \lambda = A^* \sqrt{\tfrac{u_s(x)}{2\nu_f x}} > 0, \, \delta = C^* \tfrac{u_s(x)}{2\nu_f x} < 0, \, K = \tfrac{k_0 \nu_f x_0}{U_0},$$
$$\Pr = \tfrac{\nu_f (\rho C_p)_f}{k_f}, \; R = \tfrac{4\sigma^* T_\infty^3}{k^* k_f}, \; Q = \tfrac{2Q_0 x}{u_s(x)(\rho C_p)_f}.$$

In this study, the quantities of practical interest are skin friction coefficient

C_f and local Nusselt number Nu, which are defined as

$$C_f = \frac{\tau_w}{\rho_f u_s^2/2}, \;\; Nu = \frac{x q_w}{k_f \left(T_w - T_\infty\right)}, \tag{15}$$

$$\text{where } \; \tau_w = \mu_{nf} \left(\frac{\partial u}{\partial y}\right)_{y=0}, \; q_w = -k_{nf} \left(\frac{\partial T}{\partial y} + q_r\right)_{y=0} \tag{16}$$

Substituting equation (11) into (15) and (16), we get

$$Re_x^{1/2} C_f = \sqrt{2} \frac{\mu_{nf}}{\mu_f} f''(0), \;\; Re_x^{-1/2} Nu = -\frac{1}{\sqrt{2}} \left(\frac{k_{nf}}{k_f} + \frac{4}{3} R\right) \theta'(0), \tag{17}$$

Where $Re_x = \frac{u_s |x|}{\nu_f}$ is the local Reynolds number based on the stretching velocity $u_s(x)$.

3 Computational procedure

The governing ordinary differential Equations (12)–(13) and the boundary condition (14) are solved numerically by employing a R-K fourth order method along with shooting method. Primarily, the set of coupled non-linear ODE's (12)–(13) are rehabilitated into a system of first order differential equations is as follows:

$$\left.\begin{array}{l} f = \; y_1, \;\; f' = \; y_2, \quad f'' = \; y_3, \;\; \theta = \; y_4, \;\; \theta' = \; y_5, \\ a_1 = 1 - \phi + \phi \frac{\rho_{CNT}}{\rho_f}, \;\; a_2 = (1-\phi) + \phi \frac{(\rho C_p)_{CNT}}{(\rho C_p)_f}, \;\; b = (1-\phi)^{2.5}. \end{array}\right\} \tag{18}$$

$$f''' = b a_1 \left[2n f'^2 - (n-1) f f''\right] + 2M \sin^2 \xi \; f' + \frac{2K}{(1-\phi)^{2.5}} f', \tag{19}$$

$$\theta'' = \left(-\Pr Q\theta + \Pr a_2 \left(2mf'\theta - (n-1)f\theta'\right)\right) / \left(\frac{k_{nf}}{k_f} + \frac{4}{3}R\right). \tag{20}$$

In the beginning, the BVP (boundary value problem) has been changed into IVP (initial value problem). By means of substitutions described in Eq. 18, we arrive with the following first order system of ordinary differential equations:

$$\begin{pmatrix} y_1' \\ y_2' \\ y_3' \\ y_4' \\ y_5' \end{pmatrix} = \begin{pmatrix} y_2 \\ y_3 \\ ba_1 \left[2ny_2^2 - (n-1)\, y_1 y_3\right] + 2M \sin^2 \xi \; y_2 + \frac{2K}{(1-\phi)^{2.5}} y_2 \\ y_5 \\ \left(-\Pr Q y_4 + \Pr a_2 \left(2m y_2 y_4 - (n-1) y_1 y_5\right)\right) / \left(\frac{k_{nf}}{k_f} + \frac{4}{3}R\right) \end{pmatrix} \tag{21}$$

Initial conditions are as follows

$$\begin{pmatrix} y_1(0) \\ y_2(0) \\ y_3(0) \\ y_4(0) \\ y_5(0) \end{pmatrix} = \begin{pmatrix} 0 \\ -1 - \delta s_1 - \lambda s_2 \\ s_1 \\ 1 \\ s_3 \end{pmatrix} \tag{22}$$

In order to solve the IVP, the values for $f''(0)$ and $\theta'(0)$ are needed but no such values are given prior to the computation. The initial guess values of

$f''(0)$ and $\theta'(0)$ are considered and fourth order Runge–Kutta (R–K) method is applied to solve the numerical solution. The values of $f''(0)$ and $\theta'(0)$ so found at the far field boundary condition $\eta_\infty(20)$ have been associated with the given boundary conditions (22). The step-size is taken as $\Delta\eta = 0.01$ and accuracy to the fifth decimal place as the criterion of convergence. Appropriate values of unknown initial conditions s_1 s_2 and $s_3$are approximated through Newton's method until boundary conditions $f'(\eta) \to 0$, $\theta(\eta) \to 0$ as $\eta \to \infty$ are satisfied. Computations are carried out using mathematics software MATLAB. End of boundary layer region i.e., when $\eta \to \infty$ to each group of parameters, is determined when the values of unknown boundary conditions at $y = 1$ do not change to a successful loop with error $< 10^{-6}$. Table 2 shows the validation of the present results with the published papers. We found the reasonable agreement.

4 Final outcomes and discourse of results

The effects of aligned thermal radiation, porous medium, and magnetic field on an electrically conducting flow of CNTS with base water (Seawater, blood, ethylene glycol) Nanofluid over a moving extensible surface with second-order velocity slip and heat generation/absorption is examined. To study the

effects of porosity parameter, second-order velocity slip, first order velocity slip, magnetic parameter, Prandtl number, radiation parameter and heat generation/absorption at the surface on the fluid velocity, fluid temperature, skin friction coefficient and local Nusselt number. For numerical calculations, we fixed the values of non-dimensional parameters as $\delta = -0.5,\ n = 0.6,$ $\lambda = 0.5,\ M = 1.0,\ K = 0.5,\ \phi = 0.2,\ Pr = 7.2,\ R = 1.0,\ \xi = \pi/4,\ Q = 0.2$ and $m = 10$. These values have been not diverse all through the study apart from the values showed in figures.

Fig. 2 outline the impact of magnetic field parameter on the velocity profile. It is clear that the magnetic parameter M increases from $M = 0$ to $M > 0$ results in a strong reduction in velocity for both SWCNT and MWCNT because of presence in an electrically conducting fluid familiarize with retarding body force acting transversely to the direction of the applied magnetic field. It is shown in Fig. 3 the effect of porosity parameter on velocity profile. Higher values of the porosity parameter correspond to lower velocity for both cases due to K (porosity parameter) is dependent upon the k_1 (permeability). An increment in K results in lower k_1 as they are inversely proportional, this lower k_1 instigates a reduction in velocity. Fig. 4 impact the aligned angle (ξ) on the velocity profile. It can be detected

that the expansion in ξ diminishes the velocity profile for both SWCNT and MWCNT. The explanation for this conduct is expanded in aligned angle (ξ) causes to strengthen the magnetic field. It declines the velocity boundary layer thickness. The effect of second-order slip and first-order slip on velocity profile shown in Figs. 5 and 6. We have seen that large values of second-order slip velocity parameter and first-order slip velocity parameter corresponds to high and lower velocities respectively due to stretching velocity is partially transferred to the fluid.

Figs. 7 and 8 demonstrates the impact of volume fraction (ϕ) on the velocity and temperature profile. it is inferred that as the nanoparticle volume fraction expands the nanofluid velocity increases for both SWCNT and MWCNT. Fig. 9 shows that the heat generation/absorption (Q) on the thermal field. Thermal field and its thickness layer are enhanced for larger Q. Here $Q > 0$ represents heat generation variable and $Q < 0$ represents heat absorption. Obviously in case of heat generation process more heat is delivered to working liquid which results in the increment of thermal field. Radiation parameter R on temperature is described in Fig. 10. It is detected that thermal field and boundary layer thickness are increased via R. Indeed, radiation parameter is contrarily corresponding to mean absorption coeffi-

cient. A higher value of radiation parameter leads to decay k^* which results in temperature improvement.

Figs. 11 – 15 shows the change in skin friction and local Nusselt number with governing parameters M,λ, δ, R, and Q for seawater-CNTs, blood-CNTs and ethylene glycol-CNTs. Fig. 11 represent the impact of magnetic field parameter with nanoparticle volume fraction on skin friction coefficient. It is clear that the magnetic parameter M increases from $M = 0$ (hydrodynamic) to $M > 0$ (hydromagnetic) brings about a strong reduction in skin friction coefficient because of presence in an electrically conducting fluid familiarize with retarding body force acting transversely to the direction of the applied magnetic field. The effects of first and second order velocity slips with nanoparticle volume fraction on skin friction coefficient are illustrated in Figs. 12 and 13 respectively. It is observed that the increase of first-order velocity slip parameter expands the skin friction coefficient. It is also noted that the increase of second-order velocity slip decreases the skin friction coefficient. Radiation parameter R with nanoparticle volume fraction on the local Nusselt number is portrayed in Fig. 14. It is observed that local Nusselt number increases via R. Fig. 15 shows that the heat generation/absorption (Q) with nanoparticle volume fraction on the local Nusselt number. the local

Nusselt number decreases for larger Q. Here $Q > 0$ represents heat generation variable and $Q < 0$ represents heat absorption coefficient. Naturally, in terms of heat generation process there is a lot of heat delivered in the working fluid that increases the local Nusselt number. From the above graphical results, we have concluded that the local Nusselt number is greater for ethylene glycol-CNTs whereas lessor for seawater-CNTs. The influences of M, K and n on the stream lines are revealed in Figs. 16 – 18. From these figures, we inferred that, the stream line $\psi = 0$ meets the wall $\eta = 0$. Also, the influence of the stream lines are symmetric about the Moreover, the stream lines are closer to the surface wall when lower values of M, K and n and the stream lines are far away to the surface wall higher values of M, K and n.

5 Conclusions

The study of blood flow through the stenosed arteries is considered one of the most serious physical problems because the development and cause of many arterial diseases are related to the nature of the blood flow and the deformity of the arterial wall, which leads to the development of various arterial diseases. Arterial stenosis or narrowing is most often caused by atheroma, which is the deposition of fibrous and fat in the arterial lumen. Inspired by

these applications,the present paper works to analyze the influences of the aligned magnetic field on the boundary layer flow over a stretching sheet in the presence of carbon nanotubes through a porous medium. This model designed and analyzed in this study is useful for clinicians, hematologists, and biomedical engineers as it provides some insight into understanding the physiological state of blood flow in narrow permeable blood vessels accounting external magnetic field and heat transfer effects.

In addition to this, the radiator fluid in an automobile is a mixture of water and ethylene glycol. It is used for heat transfer applications in automobiles limit the performance enhancement and compactness of the heat exchangers. There is a bright future for CNTs-based layers in water purification and desalination technology. The composite electrode with CNTs was the most suitable for the removal of NaCl due to its highly efficient regeneration characteristic, low energy- consumption and high removal characteristic. And also, SWCNTs-seawater is expected to exhibit better heat transfer properties. The main conclusions of the reachable study are the velocity and boundary layer thickness lower with rising values of first order velocity slip and the opposite with rising values of second-order velocity slip. In the velocity profile, the values of single-wall carbon nanotubes are lesser than

the multi-wall carbon nanotubes whereas the reverse trend is observed in the temperature profile. The local Nusselt decrease for increasing the values of heat generation/absorption whereas the reverse trend is observed in radiation parameter. From graphical results, we can conclude that the velocity is greater for ethylene glycol-CNTs whereas lessor for seawater-CNTs. From graphical results, we concluded that ethylene glycol-CNTs transfer more heat when compared to the Blood-CNT and seawater-CNTs.

REFERENCES

Akbara, N.S., Tripathi, D., and Khan, Z.H., Numerical Investigation of Cattanneo-Christov Heat Flux in Cnt Suspended Nanofluid Flow Over a Stretching Porous Surface with Suction and Injection, *Discrete and Continuous Dynamical Systems - Series S*, vol. **11**, no. 4, pp. 583-594, 2018.

Aly, E.H., Dual Exact Solutions of Graphene Water Nano Fluid Flow Over Stretching/Shrinking Sheet with Suction/Injection and Heat Source/Sink: Critical Values and Regions with Stability, Powder *Technology*, vol. **342**, pp.528-544, 2019.

Aly, E.H. and Sayed, H.M., Magnetohydrodynamic and Thermal Radiation Effects on the Boundary-Layer Flow due to a Moving Extensible Surface with the Velocity Slip Model: A Comparative Study of Four Nanofluids, *J. of Magnetism and Magnetic Materials*, vol. **422**, pp. 440-451, 2017.

Bala Anki Reddy, P., Magnetohydrodynamic Flow of a Casson Fluid Over an Exponentially Inclined Permeable Stretching Surface with Thermal Radiation and Chemical Reaction, *Ain Shams Eng. J.*, vol. **7**, pp. 593-602, 2016.

Besthapu, P., Haq, R.U., Bandari, S., and Al-Mdallal, Q.M., Mixed Convection Flow of Thermally Stratified MHD Nanofluid Over an Exponentially Stretching Surface with Viscous Dissipation Effect, *J. of the Taiwan Inst. of Chem. Eng.*, vol. **71**, pp. 307-314, 2017.

Bhatti, M.M., Abbas, T., Rashidi, M.M., Ali, M.E.S., and Yang, Z., Entropy Generation on MHD Eyring-Powell Nanofluid Through a Permeable Stretching Surface, *Entropy*, vol. **18**, no. 6, pp. 114, 2016.

Bhatti, M.M. and Rashidi, M.M., Numerical simulation of entropy generation on MHD Nanofluid towards a Stagnation Point Flow over a Stretching Surface, *Int. J. Appl. Comput. Math*., vol. **3**, no. 3, pp. 2275-2289, 2017.

Buongiorno, J., Convective Transport in Nanofluids, *J. of Heat Transfer*, vol. **128**, no. 3, pp. 240-250, 2006.

Chamkha, A.J., Rashad, A.M., Armaghani, T., and Mansour, M.A., Effects of Partial Slip on Entropy Generation and MHD Combined Convection in a Lid-Driven Porous Enclosure Saturated with a Cu-water Nanofluid, *J. of Thermal Analysis and Calorimetry*, vol. **132**, no. 2, pp. 1291-1306, 2018.

Ellahi, R., Hassan, M., and Zeeshan, A., Study of Natural Convection MHD Nanofluid by Means of Single and Multi-Walled Carbon Nanotubes Suspended in a Salt-Water Solution, *IEEE Transactions on Nanotechnology*, vol. **14**, no. 4, pp. 726-734, 2015.

Gaffney, A.M., Santos-Martinez, M.J., Satti, A., Major, T.C., Wynne, K.J., Gunko, Y.K., Annich, G.M., Elia, G., and Radomski, M.W., Blood Biocompatibility of Surface-Bound Multi-Walled Carbon Nanotubes, *Nanomedicine: Nanotechnology, Biology and Medicine*, vol. **11**, no. 1, pp. 39-46, 2014.

Hakeem, A.A., Ganesh, N.V., and Ganga, B., Magnetic Field Effect on Second Order Slip Flow of Nanofluid Over a Stretching/ Shrinking Sheet with Thermal Radiation Effect, *J. of Magnetism and Magnetic Materials*, vol. **381**, pp. 243-257, 2015.

Hayat, T., Imtiaz, M., and Alsaedi, A., Impact of Magnetohydrodynamics in Bidirectional Flow of Nanofluid Subject to Second Order Slip Velocity and Homogeneous-heterogeneous Reactions, *J. of Magnetism and Magnetic Materials*, vol. **395**, pp. 294-302, 2015.

Hayat, T., Waqas, M., Khan, M.I., and Alsaedi, A., Impacts of Constructive and Destructive Chemical Reactions in Magnetohydrodynamic (MHD) Flow of Jeffrey Liquid Due to Nonlinear Radially Stretched Surface, *J. of Molecular Liquids*, vol. **225**, pp. 302-310, 2017.

He, H., Pham-Huy, L.A., Dramou, P., Xiao, D., Zuo, P., and Pham-Huy, C., Carbon Nanotubes: Applications in Pharmacy and Medicine, *BioMed Research Int.*, vol. **2013**, pp. 112, 2013. DOI: 10.1155/2013/578290

Ihsanullah, I., Carbon Nanotube Membranes for Water Purification: Developments, Challenges, and Prospects for the Future, Separation and Purification Technology, vol. **209**, pp. 307-337, 2019.

Kalaivanan, R., Ganga, B., Vishnu Ganesh, N., and Abdul Hakeem, A.K., Effect of Elastic Deformation on Nano-Second Grade Fluid Flow Over a Stretching Surface, *Frontiers in Heat and Mass Transfer*, vol. **10**, no. 20, pp. 19, 2018.

Kandasamy, R., bt Adnan, N.A., Abbood, J.A.A., Kamarulzaki, M., and Saifullah, M., Electric Field Strength On Water Based Aluminum Alloys Nanofluids Flow Up a Non-Linear Inclined Sheet, *Eng. Sci. and Tech., an Int. J.*, vol. **22**, no. 1, pp. 229-236, 2019.

Kandasamy, R., Muhaimin, I., and Mohammad, R., Single Walled Carbon Nanotubes on MHD Unsteady Flow Over a Porous Wedge with Thermal Radiation with Variable Stream Conditions, *Alexandria Eng. J.*, vol. **55**, no. 1, pp. 275-285, 2016.

Kandasamy, R., Vignesh, V., Kumar, A., Hasan, S.H., and Isa, N.M., Thermal Radiation Energy Due To SWCNTs On MHD Nanofluid Flow in the Presence of Seawater/Water: Lie Group Transformation, *Ain Shams Eng. J.*, vol. **9**, no. 4, pp. 953-963, 2018.

Khalid, A., Khan, I., Khan, A., Shafie, S., and Tlili, I., Case Study of MHD Blood Flow in a Porous Medium with CNTs and Thermal Analysis, *Case Studies in Thermal Eng.*, vol. **12**, pp. 374-380, 2018.

Kudenatti, R.B., Awati, V.B., and Bujurke, N.M., Approximate Analytical Solutions of a Class of Boundary Layer Equations Over Nonlinear Stretching Surface, *Appl. Math. and Computation*, vol. **218**, no. 6, pp. 2952-2959, 2011.

Kuiken, H.K., On Boundary Layers in Fluid Mechanics That Decay Algebraically Along Stretches of Wall That are not Vanishingly Small, *IMA J. of Appl. Math. (Institute of Math. and Its Applications)*, vol. **27**, no. 4, pp. 387-405, 1981.

Liao, S., On the Homotopy Analysis Method for Nonlinear Problems, *Appl. Math. and Computation*, vol. **147**, no. 2, pp. 499-513, 2004.

Lu, D., Ramzan, M., Ul Huda, N., Chung, J.D., and Farooq, U., Non-Linear Radiation Effect on MHD Carreau Nanofluid Flow Over a Radially Stretching Surface with Zero Mass Flux at the Surface, *Scientific Reports*, vol. **8**, no. 1, pp. 117, 2018.

Mabood, F. and Mastroberardino, A., Melting Heat Transfer on MHD Convective Flow Of A Nanofluid Over a Stretching Sheet with Viscous Dissipation and Second Order Slip, *J. of the Taiwan Inst. of Chem. Eng.*, vol. **57**, pp. 62-68, 2015.

Makinde, O.D., Mabood, F., Khan, W.A., and Tshehla, M.S., MHD Flow of a Variable Viscosity Nanofluid Over a Radially Stretching Convective Surface with Radiative Heat, *J. of Molecular Liquids*, vol. **219**, pp. 624-630, 2016.

Mohammdien, S.A., Raslan, K., Abdel-wahed, M.S., and Abedel-aal, E.M., KKL-Model of MHD CuO-nanofluid Flow Over a Stagnation Point Stretching Sheet with Nonlinear Thermal Radiation and Suction/Injection, *Results in Phys.*, vol. **10**, pp. 194-199, 2018.

Mustafa, M., Hayat, T., and Alsaedi, A., Heat Transfer In Oldroyd-B Fluid Flow due to an Exponentially Stretching Wall Utilizing Cattaneo-Christov Heat Flux Model, *J. of the Brazilian Soc. of Mech. Sci. and Eng.*, vol. **40**, no. 191, pp. 19, 2018. DOI: 10.1007/s40430-018-1132-6

Muthucumaraswamy, R., Effects of a Chemical Reaction on a Moving Isothermal Vertical Surface with Suction, *Acta Mechanica*, vol. **155**, pp. 6570, 2002.

Nasir, S., Islam, S., Gul, T., Khan, Z.S., Khan, M.A., Khan, W., Khan, A.Z., and Khan, S., Three Dimensional Rotating Flow Of MHD Single Wall Carbon Nanotubes Over a Stretching Sheet in Presence of Thermal Radiation, *Appl. Nanoscience*, vol. **8**, pp. 118, 2018.

Reddy, P.B.A. and Reddy, N.B., Finite Difference Analysis of Radiation Effects on Unsteady MHD Flow of a Chemically Reacting Fluid with Time-Dependent Suction, Int. J. of Appl. Math and Mech., vol. **7**, no. 9, pp. 96-105, 2011.

Reddy, P.B.A., Reddy, N.B., and Suneetha, S., Radiation Effects on MHD Flow Past an Exponentially Accelerated Isothermal Vertical Plate with Uniform Mass Diffusion in the Presence of Heat Source, *J. of Applied Fluid Mech.*, vol. **5**, no. 3, pp. 119-126, 2012.

Reddy, S.R.R. and Bala Anki Reddy, P., Bio-Mathematical Analysis for the Stagnation Point Flow Over a Non-Linear Stretching Surface with the Second Order Velocity Slip and Titanium Alloy Nanoparticle, *Frontiers in Heat and Mass Transfer*, vol. **10**, no. 13, pp. 111, 2018. DOI: 10.5098/hmt.10.13

Reddy, S.R.R., Bala Anki Reddy, P., and Suneetha, S., Magnetohydro-Dynamic Flow of Blood in a Permeable Inclined Stretching Surface with Viscous Dissipation, Non-Uniform Heat Source/Sink and Chemical Reaction, *Frontiers in Heat and Mass Transfer*, vol. **10**, no. 22, pp. 110, 2018. DOI: 10.5098/hmt.10.22

Sheikholeslami, M. and Rokni, H.B., Numerical Simulation for Impact of Coulomb Force on Nanofluid Heat Transfer in a Porous Enclosure in Presence of Thermal Radiation, *Int. J. of Heat and Mass Transfer*, vol. **118**, pp. 823-831, 2018.

Singh, G. and Chamkha, A.J., Dual Solutions for Second-Order Slip Flow and Heat Transfer on a Vertical Permeable Shrinking Sheet, *Ain Shams Eng. J.*, vol. **4**, no. 4, pp. 911-917, 2013.

Srinivas, S., Reddy, P.B.A., and Prasad, B.S.R.V., Effects of Chemical Reaction and Thermal Radiation on MHD Flow Over an Inclined Permeable Stretching Surface with Non-Uniform Heat Source/Sink: An Application to the Dynamics of Blood Flow, *J. of Mech. in Medicine and Biology*, vol. **14**, no. 5, pp. 1450067124, 2014. DOI: 10.1142/S0219519414500675

Tofighy, M.A. and Mohammadi, T., Salty Water Desalination using Carbon Nanotube Sheets, *Desalination*, vol. **258**, no. 1-3, pp. 182-186, 2010.

Turkyilmazoglu, M., Analytical Solutions to Mixed Convection MHD Fluid Flow Induced by a Nonlinearly Deforming Permeable Surface, *Comm. in Nonlinear Sci. and Num. Sim.*, vol. 63, pp. 373-379, 2018a.

Turkyilmazoglu, M., Analytical Solutions to Mixed Convection MHD Fluid Flow Induced by a Nonlinearly Deforming Permeable Surface, *Comm. in Nonlinear Sci. and Num. Sim.*, vol. **3**, pp. 373-379, 2018b.

Turkyilmazoglu, M., MHD Natural Convection in Saturated Porous Media with Heat Generation/Absorption and Thermal Radiation: Closed-Form Solutions, *Archives of Mechanics*, vol. **71**, no. 1, pp. 49-64, 2019.

Ur Rehman, F., Nadeem, S., Ur Rehman, H., and Ul Haq, R., Thermophysical Analysis for Three-Dimensional MHD Stagnation-Point Flow of Nano-Material Influenced by an Exponential Stretching Surface, *Results in Physics*, vol. **8**, pp. 316-323, 2018.

Waini, I., Ishak, A., and Pop, I., Unsteady Flow and Heat Transfer Past a Stretching-Shrinking Sheet in a Hybrid Nanofluid, *Int. J. of Heat and Mass Trans.*, vol. **136**, pp. 288-297, 2019.

Zeeshan, A., Majeed, A., and Ellahi, R., Effect of Magnetic Dipole on Viscous Ferro-Fluid Past a Stretching Surface with Thermal Radiation, *J. of Molecular Liquids*, vol. **215**, pp. 549-554, 2016.

Zhang, D., Shi, L., Fang, J., and Dai, K., Removal of NaCl from Saltwater Solution Using Carbon Nanotubes/Activated Carbon Composite Electrode, *Materials Letters*, vol. **60**, no. 3, pp. 360-363, 2006.

Zhang, L., Shi, G.Z., Qiu, S., Cheng, L.H., and Chen, H.L., Preparation of High-Flux Thin Film Nanocomposite Reverse Osmosis Membranes by Incorporating Functionalized Multi-Walled Carbon Nanotubes, *Desalination and Water Treatment*, vol. **34**, no. 1-3, pp. 19-24, 2011.

Nomenclature

u, v	velocity components in x and y directions
$B(x)$	magnetic field
U_0	characteristic velocity
T_0	characteristic temperature
B_0	uniform magnetic field
x_0	reference length scales

μ_0	magnetic permeability
M	magnetic parameter
Pr	Prandtl number
R	radiation parameter
k_1	permeability parameter
k_{CNTs}	the thermal conductivity of the CNTs
k_f	the thermal conductivity of the fluid
$k*$	Rosseland mean absorption coefficient
k_{nf}	thermal conductivity of the nanofluid
K	porosity perameter
Q	heat generation or absorption parameter
T	local temperature of the fluid
T_w	the temperature of the fluid at the wall
u_w	stretching/shrinking sheet velocity
T_∞	free stream temperature

Greek symbols

ϕ	solid volume fraction
α	thermal diffusivity coefficient
α_{CNT}	thermal diffusivity of the CNT

ρ_{CNT}	the density of the CNT
$(\rho c_p)_{CNT}$	heat capacitance of the CNT
α_{nf}	thermal diffusivity of the nanofluid
ρ_{nf}	the density of the nanofluid
μ_{nf}	dynamic viscosity of the nanofluid
$(\rho c_p)_{nf}$	heat capacitance of the nanofluid
ν_f	the kinematic viscosity of the fluid
α_f	thermal diffusivity of the fluid
μ_f	dynamic viscosity of the fluid
ρ_f	the density of the fluid friction
$(\rho c_p)_f$	heat capacitance of the fluid
ν	kinematic viscosity
μ	dynamic viscosity
σ^*	Stefan–Boltzmann constant
σ	electrical conduction
C_p	specific heat at constant pressure
θ	non-dimensional temperature
τ_w	shear stress
q_w	heat flux

Subscripts

∞	condition at free stream
nf	nanofluid
f	fluid phase
s	CNTs phase
w	condition at the wall

Superscript

$'$	Differentiation with respect to η

Table 1: Thermophysical properties of base fluids (water, blood and ethylene glycol) and CNT's (see Kandasamy et al. (2018))

Physical properties	**Base fluids**			**Nanoparticles**	
	Seawater	**Blood**	**Ethylene glycol**	**SWCNT**	**MWCNT**
$\rho\ (kg/m^3)$	1021	1063	1115	2,600	1,600
$C_p\ (J/kg\,K)$	3993	3594	2430	425	796
$k\ (W/m\,K)$	0.596	0.492	0.253	6,600	3,000

Table 2: validation of the present results when $M = \delta = \lambda = \phi = 0$.

n	Liao (2004)	Kudenatti et al. (2011)	Aly and Sayed (2017)	Present
	$f''(0)$	$n^{-1/2}f''(0)$	$f''(0)$	$f''(0)$
0.1	-0.215052		-0.2151523	-0.21510
0.3	-0.519994		-0.5199936	-0.52000
0.5	-0.744394		-0.7443950	-0.74444
0.7	-0.926891		-0.9268906	-0.92690
0.9	-1.083447		-1.0834491	-1.08340
1.5		-1.19485	-1.094850	-1.19490
2.5		-1.22896	-1.228965	-1.22900
5.0		-1.25523	-1.255231	-1.25520
10.0		-1.26849	-1.268443	-1.26850
100.0		-1.28048	-1.280475	-1.28050

FIG. 1: Physical configuration of the problem.

FIG. 2: Effect of M on $f'(\eta)$.

FIG. 3: Effect of K on $f'(\eta)$.

FIG. 4: Effect of ξ on $f'(\eta)$.

FIG. 5: Effect of δ on $f'(\eta)$.

FIG. 6: Effect of λ on $f'(\eta)$.

FIG. 7: Effect of ϕ on $f'(\eta)$.

FIG. 8: Effect of ϕ on $\theta(\eta)$.

FIG. 9: Effect of Q on $\theta(\eta)$.

FIG. 10: Effect of R on $\theta(\eta)$.

FIG. 11: Effect of M and ϕ on $Re_x^{1/2}C_f$.

FIG. 12: Effect of λ and ϕ on $Re_x^{1/2}C_f$.

FIG. 13: Effect of δ and ϕ on $Re_x^{1/2}C_f$.

FIG. 14: Effect of R and ϕ on $Re_x^{-1/2}Nu$.

FIG. 15: Effect of Q and ϕ on $Re_x^{-1/2}Nu$.

FIG. 16: streamline pattern for various values of M.

FIG. 17: streamline pattern for various values of K.

FIG. 18: streamline pattern for various values of n.

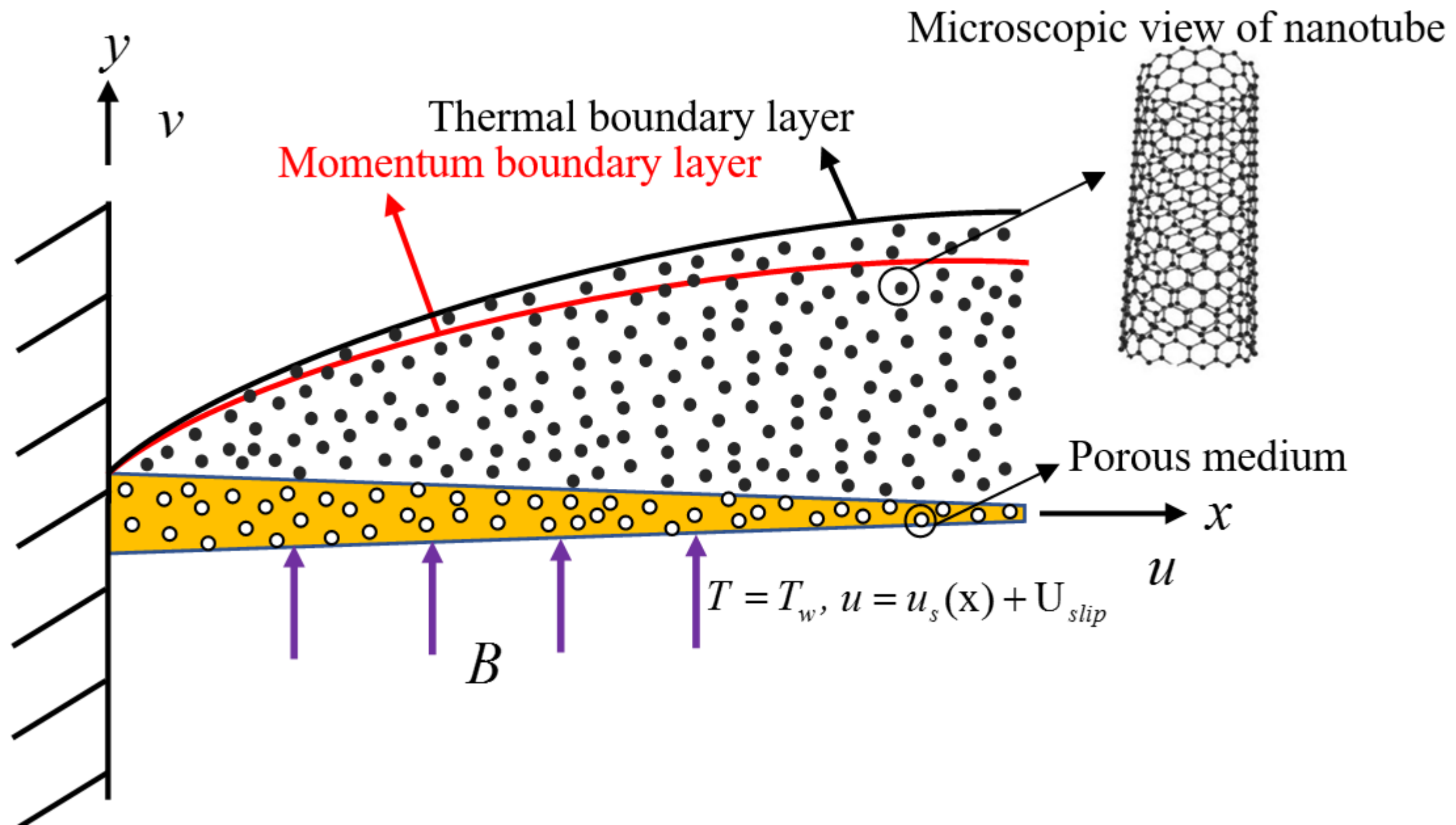
Microscopic view of nanotube
y
v
Thermal boundary layer
Momentum boundary layer
Porous medium
x
u
$T = T_w,\ u = u_s(\mathrm{x}) + \mathrm{U}_{slip}$
B

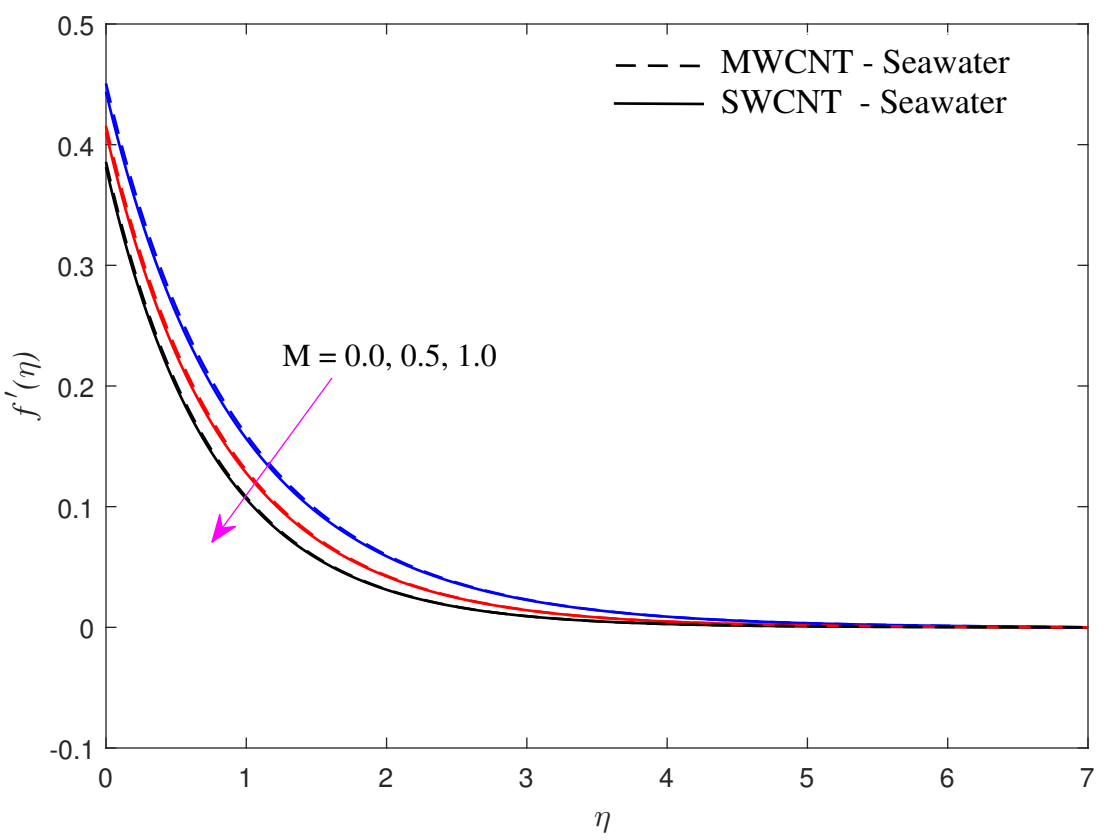
MWCNT - Seawater
SWCNT - Seawater
M = 0.0, 0.5, 1.0
$f'(\eta)$
η
0.5
0.4
0.3
0.2
0.1
0
-0.1
0
1
2
3
4
5
6
7

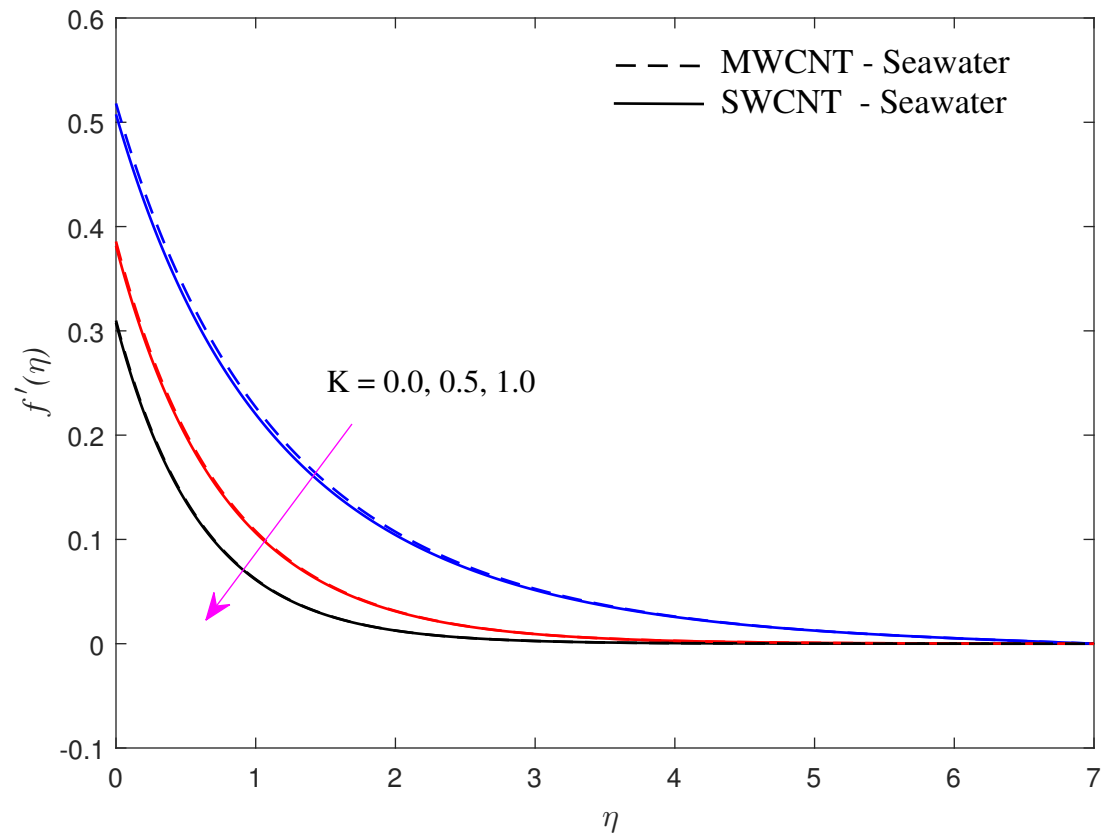
MWCNT - Seawater
SWCNT - Seawater
K = 0.0, 0.5, 1.0
$f'(\eta)$
η
0.6
0.5
0.4
0.3
0.2
0.1
0
-0.1
0
1
2
3
4
5
6
7

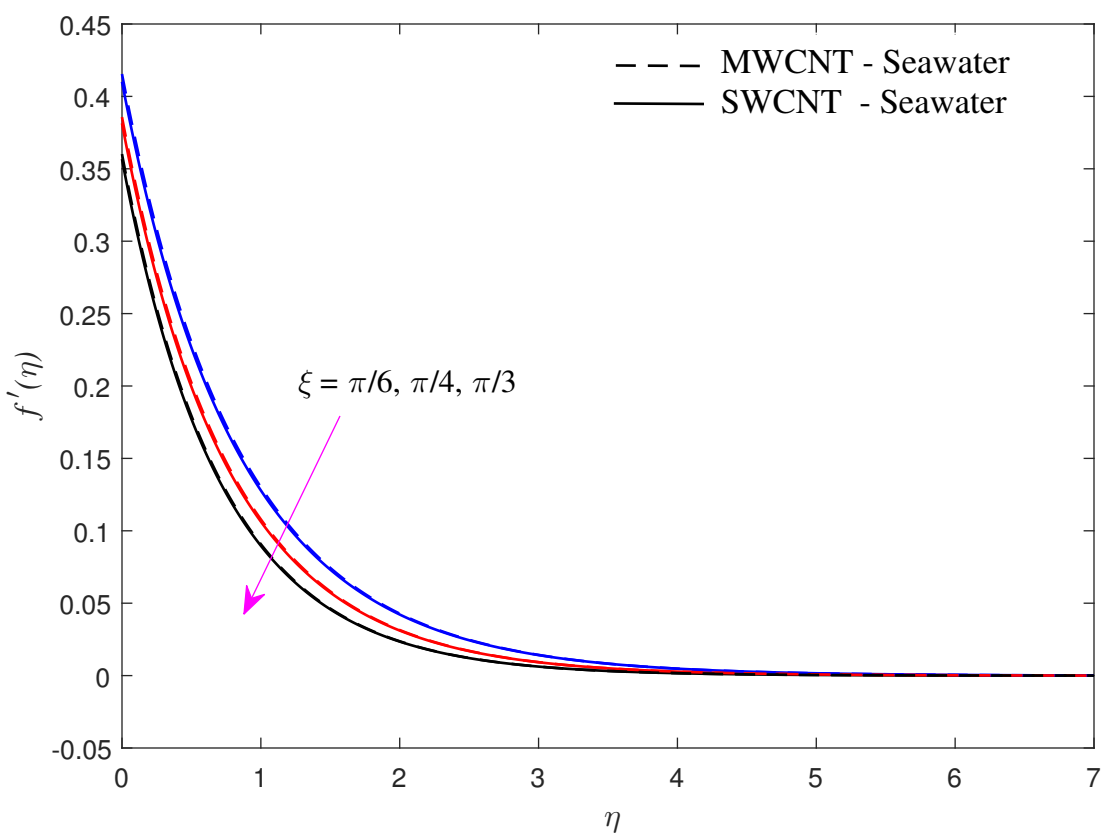
MWCNT - Seawater
SWCNT - Seawater
$\xi = \pi/6, \pi/4, \pi/3$
$f'(\eta)$
η
0.45
0.4
0.35
0.3
0.25
0.2
0.15
0.1
0.05
0
-0.05
0
1
2
3
4
5
6
7

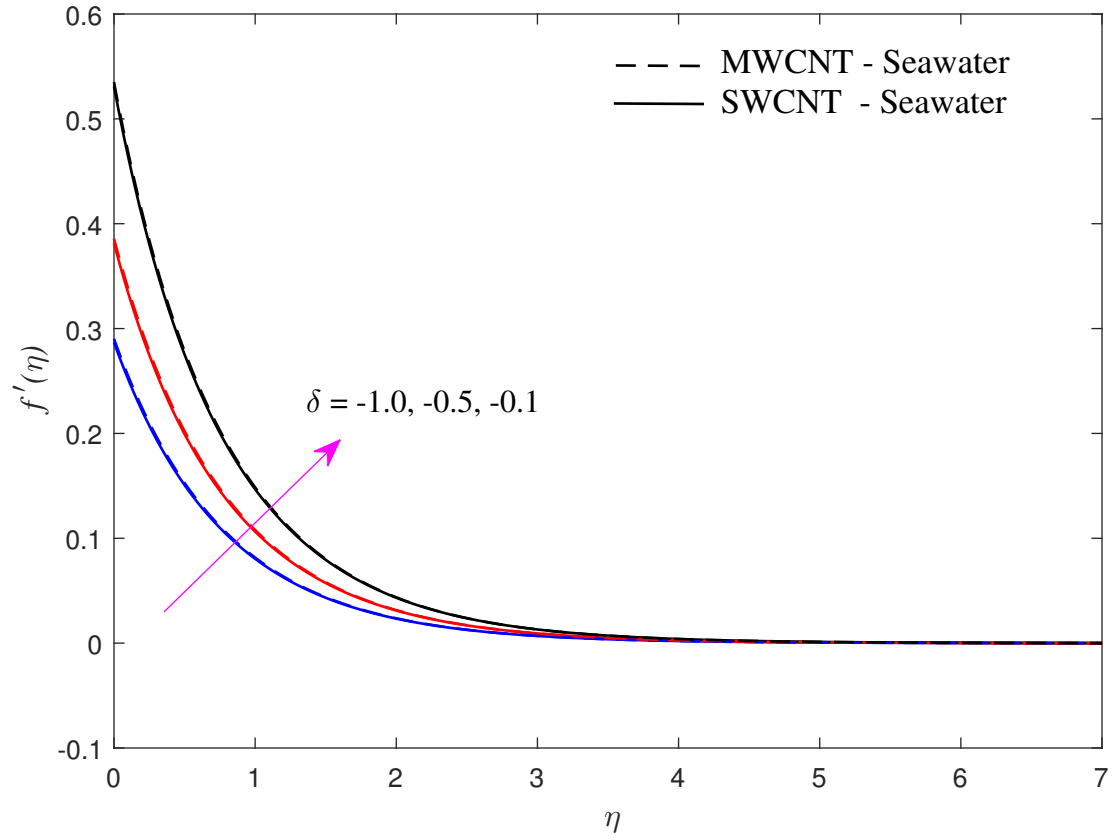
MWCNT - Seawater
SWCNT - Seawater
δ = -1.0, -0.5, -0.1
$f'(\eta)$
η
0.6
0.5
0.4
0.3
0.2
0.1
0
-0.1
0
1
2
3
4
5
6
7

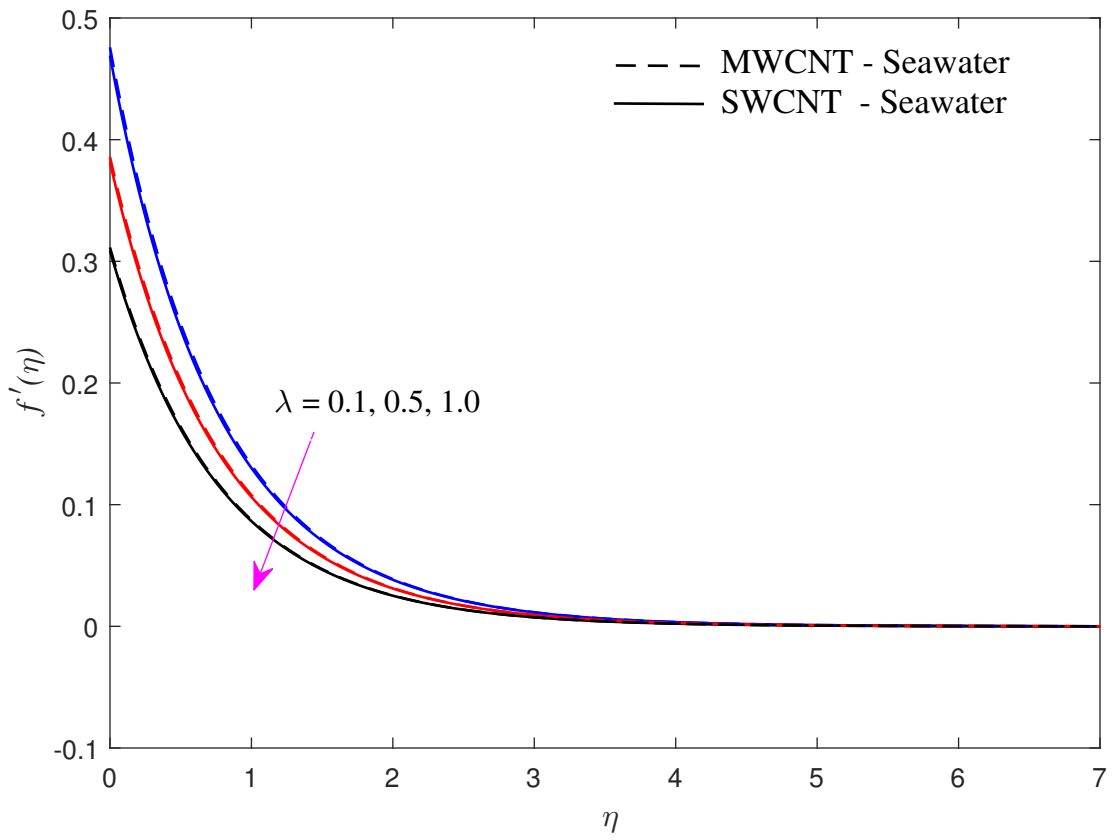
MWCNT - Seawater
SWCNT - Seawater
$\lambda = 0.1, 0.5, 1.0$
$f'(\eta)$
η
0.5
0.4
0.3
0.2
0.1
0
-0.1
0
1
2
3
4
5
6
7

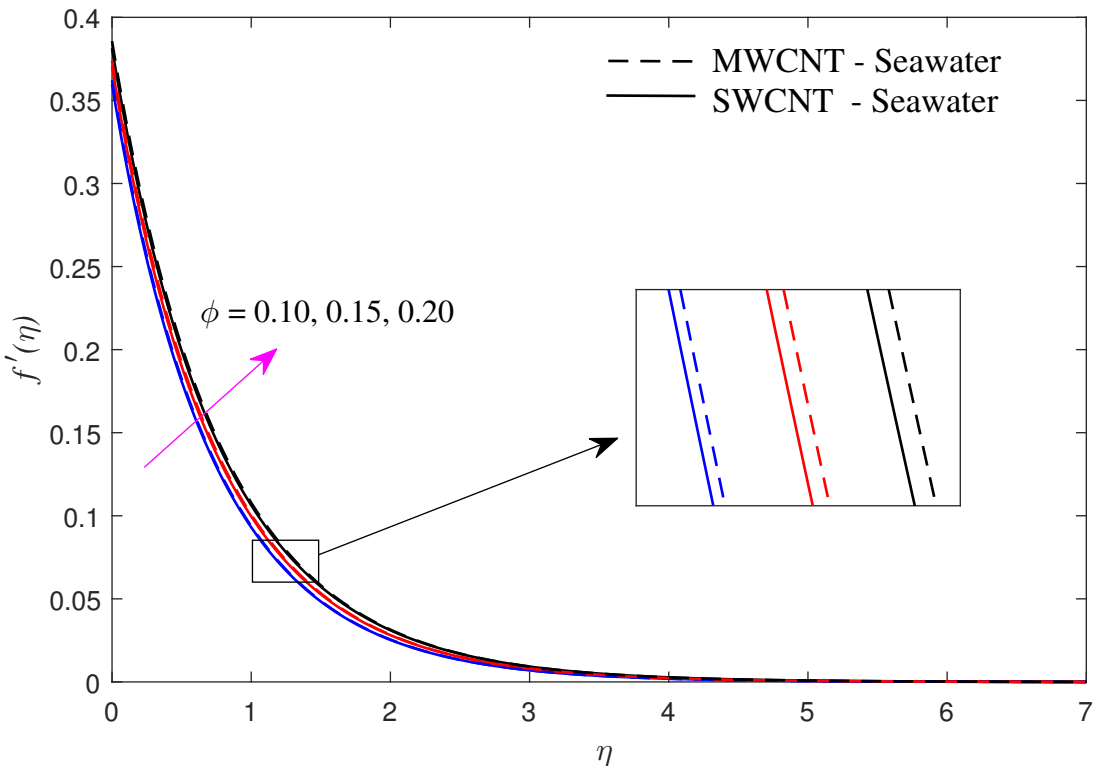
MWCNT - Seawater
SWCNT - Seawater
ϕ = 0.10, 0.15, 0.20
$f'(\eta)$
η
0.4
0.35
0.3
0.25
0.2
0.15
0.1
0.05
0
0
1
2
3
4
5
6
7

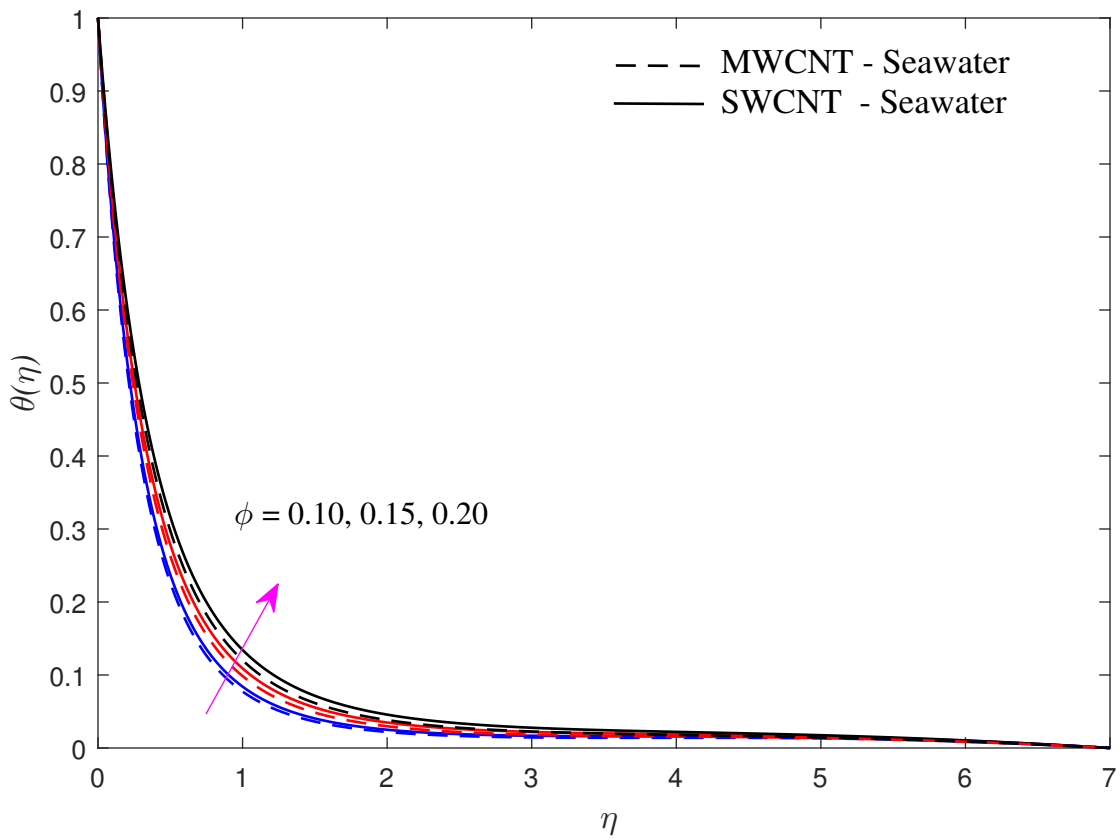
MWCNT - Seawater
SWCNT - Seawater
ϕ = 0.10, 0.15, 0.20
$\theta(\eta)$
η
0
0.1
0.2
0.3
0.4
0.5
0.6
0.7
0.8
0.9
1
0
1
2
3
4
5
6
7

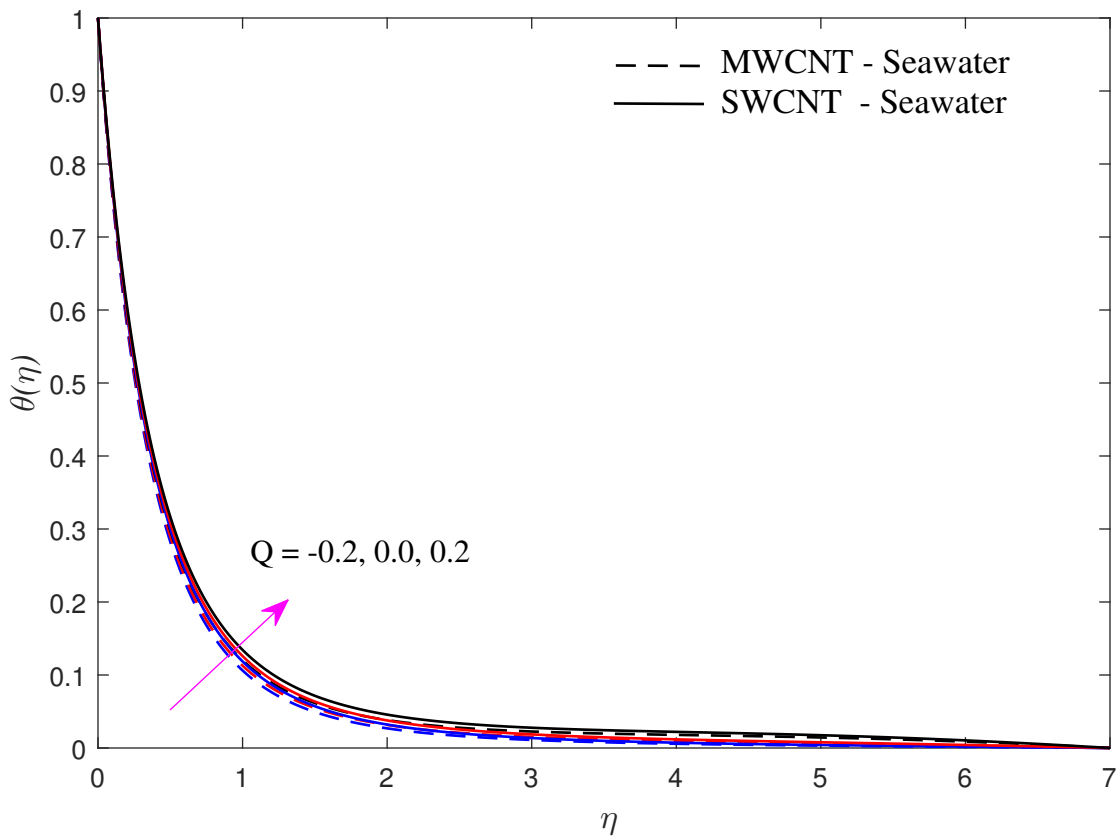
MWCNT - Seawater
SWCNT - Seawater
Q = -0.2, 0.0, 0.2
$\theta(\eta)$
η
0
0.1
0.2
0.3
0.4
0.5
0.6
0.7
0.8
0.9
1
0
1
2
3
4
5
6
7

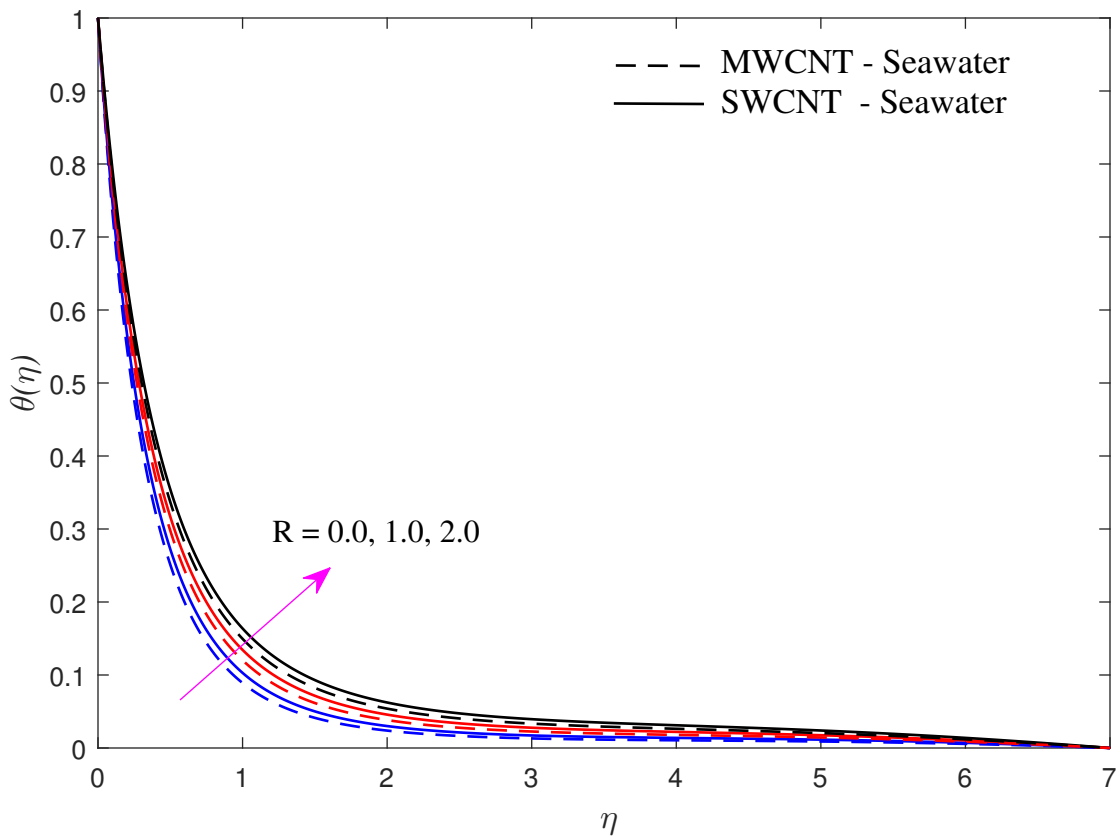
MWCNT - Seawater
SWCNT - Seawater
R = 0.0, 1.0, 2.0
$\theta(\eta)$
η
0
0.1
0.2
0.3
0.4
0.5
0.6
0.7
0.8
0.9
1
0
1
2
3
4
5
6
7

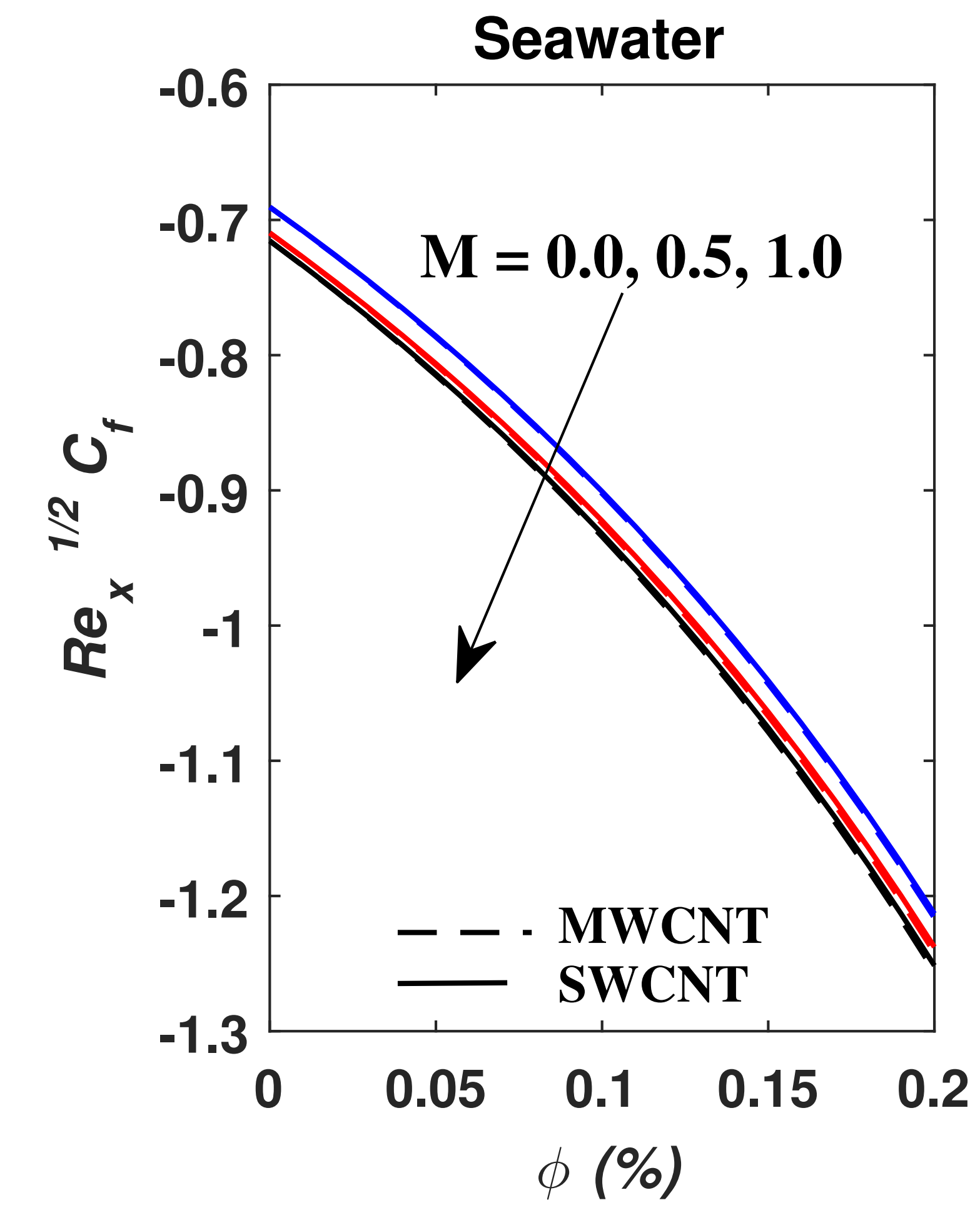
Seawater
-0.6
-0.7
-0.8
-0.9
-1
-1.1
-1.2
-1.3
$Re_x^{1/2} C_f$
M = 0.0, 0.5, 1.0
MWCNT
SWCNT
0
0.05
0.1
0.15
0.2
ϕ (%)

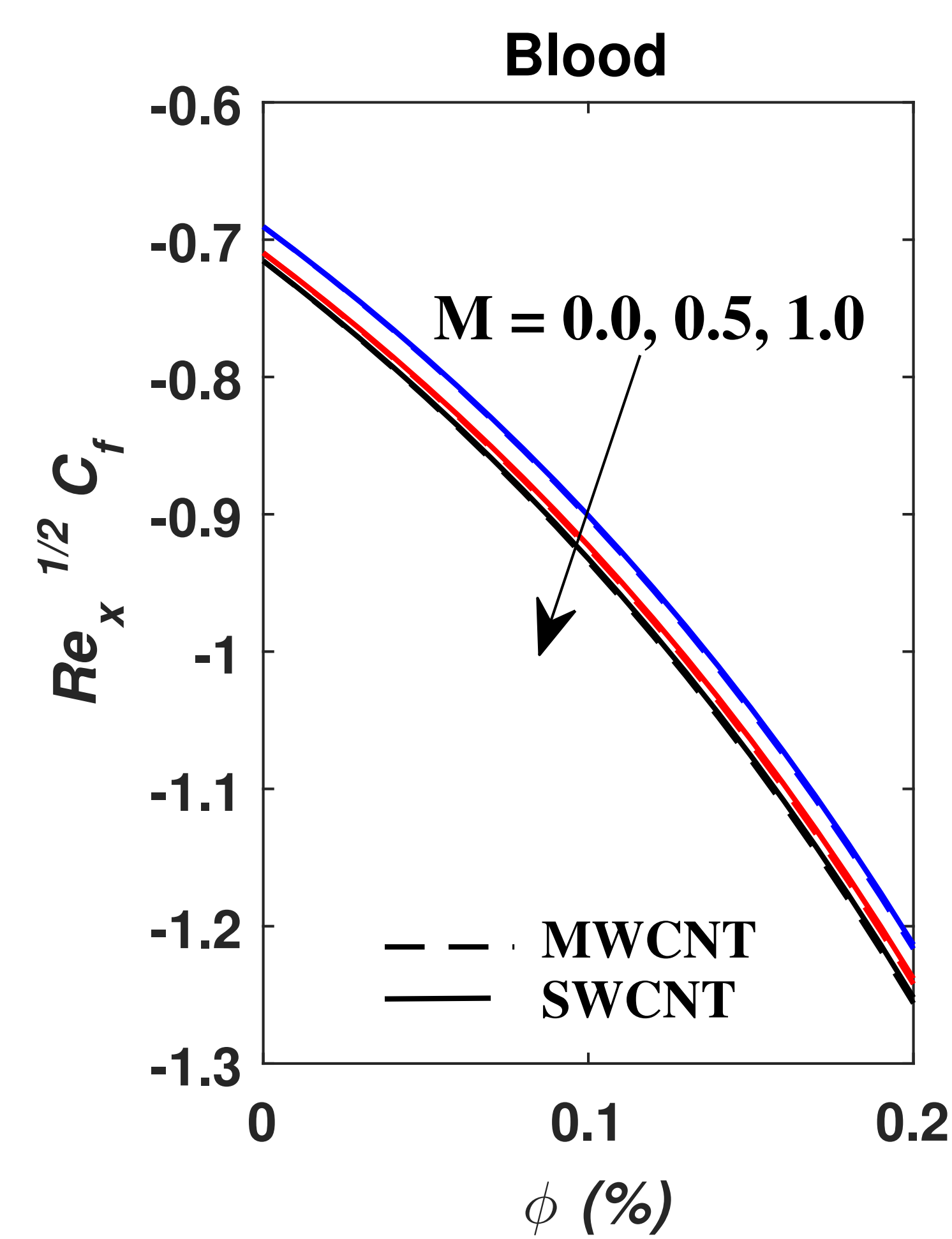
Blood
-0.6
-0.7
-0.8
-0.9
-1
-1.1
-1.2
-1.3
0
0.1
0.2
$Re_x^{1/2} C_f$
ϕ (%)
M = 0.0, 0.5, 1.0
MWCNT
SWCNT

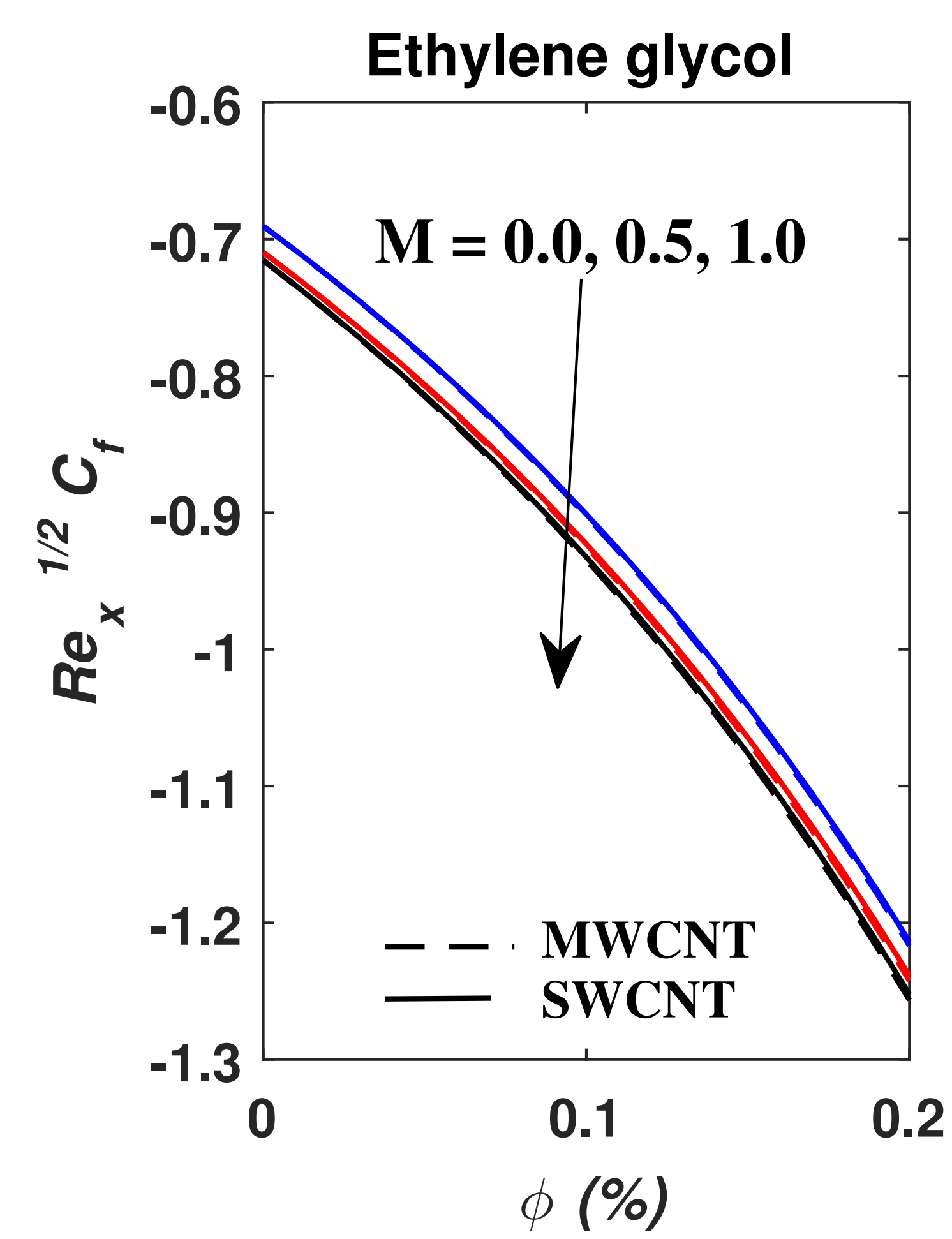
Ethylene glycol
M = 0.0, 0.5, 1.0
MWCNT
SWCNT
$Re_x^{1/2} C_f$
ϕ (%)
-0.6
-0.7
-0.8
-0.9
-1
-1.1
-1.2
-1.3
0
0.1
0.2

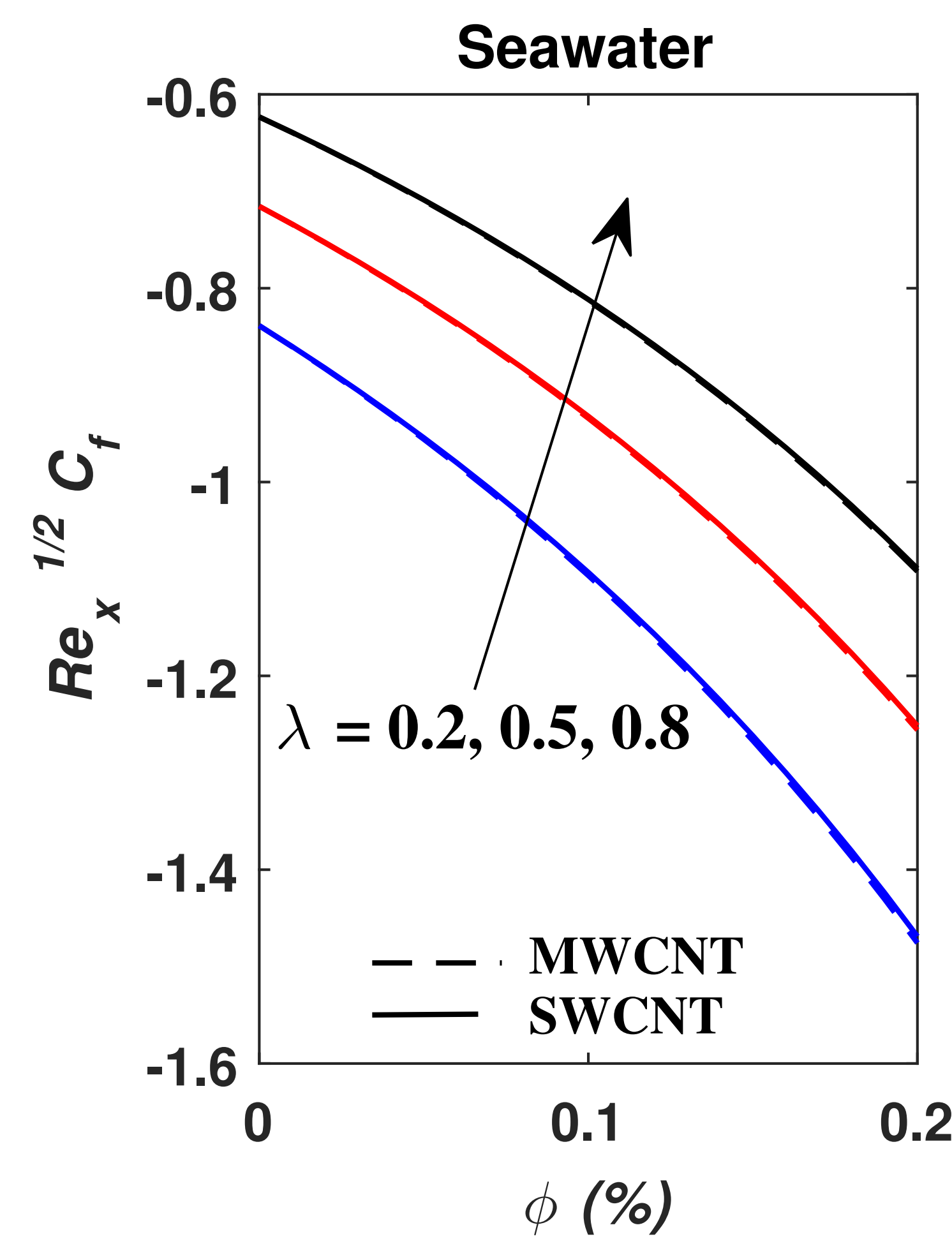
Seawater
-0.6
-0.8
-1
-1.2
-1.4
-1.6
$Re_x^{1/2} C_f$
$\lambda = 0.2, 0.5, 0.8$
MWCNT
SWCNT
0
0.1
0.2
ϕ (%)

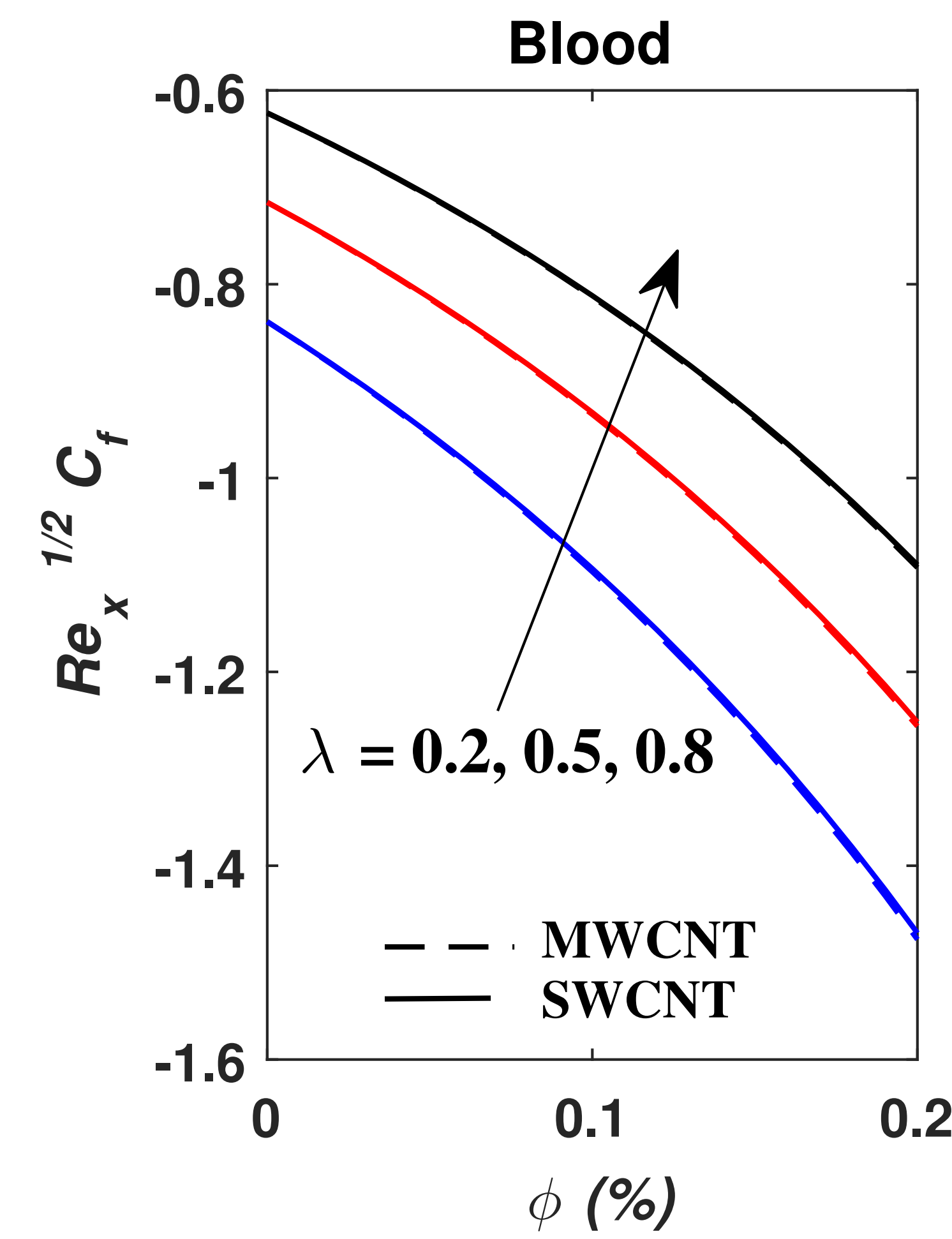
Blood
-0.6
-0.8
-1
-1.2
-1.4
-1.6
0
0.1
0.2
$Re_x^{1/2} C_f$
ϕ (%)
λ = 0.2, 0.5, 0.8
MWCNT
SWCNT

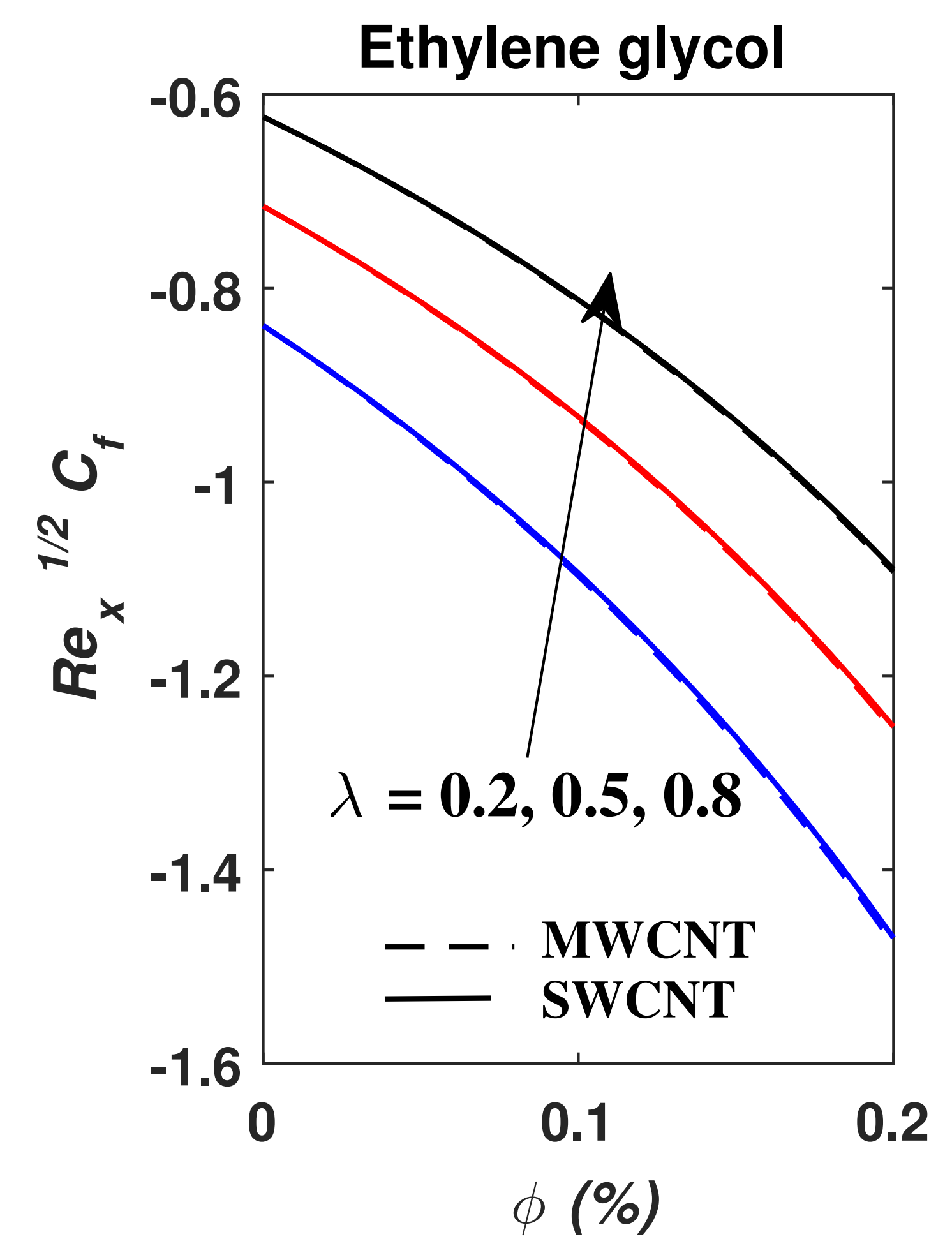
Ethylene glycol
-0.6
-0.8
-1
-1.2
-1.4
-1.6
$Re_x^{1/2} C_f$
0
0.1
0.2
ϕ (%)
$\lambda = 0.2, 0.5, 0.8$
MWCNT
SWCNT

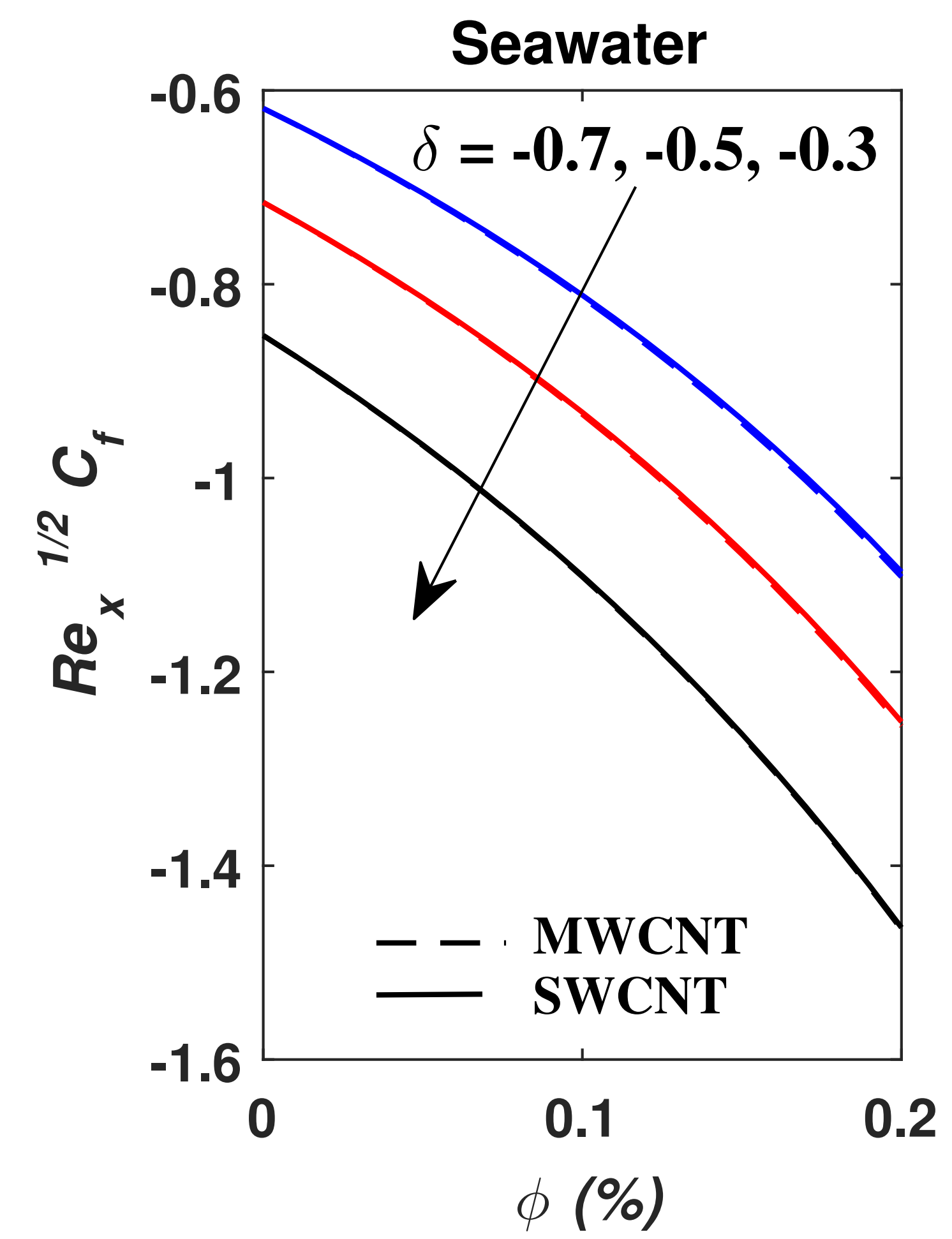
Seawater
-0.6
-0.8
-1
-1.2
-1.4
-1.6
$Re_x^{1/2} C_f$
δ = -0.7, -0.5, -0.3
MWCNT
SWCNT
0
0.1
0.2
ϕ (%)

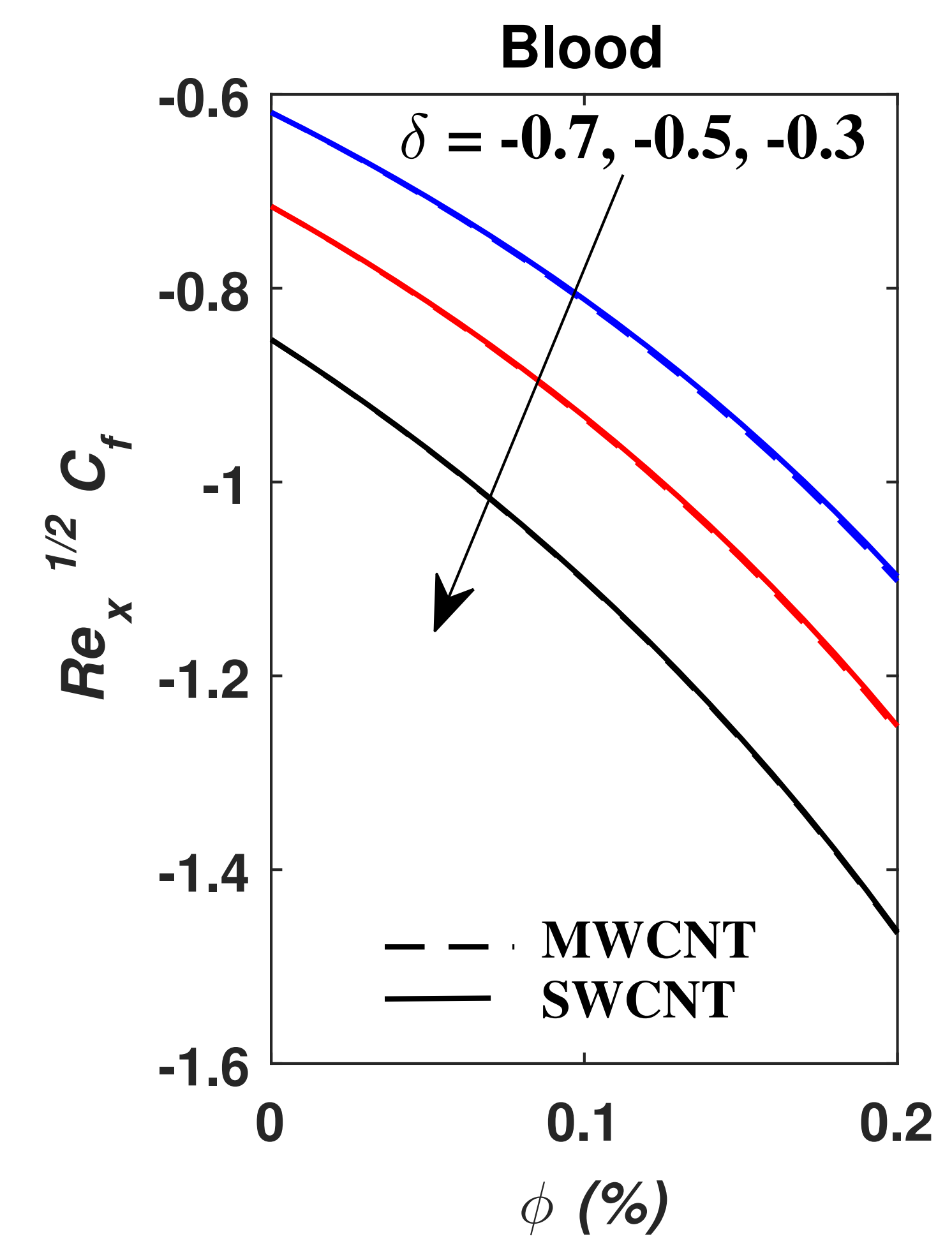
Blood
δ = -0.7, -0.5, -0.3
MWCNT
SWCNT
$Re_x^{1/2} C_f$
ϕ (%)
-0.6
-0.8
-1
-1.2
-1.4
-1.6
0
0.1
0.2

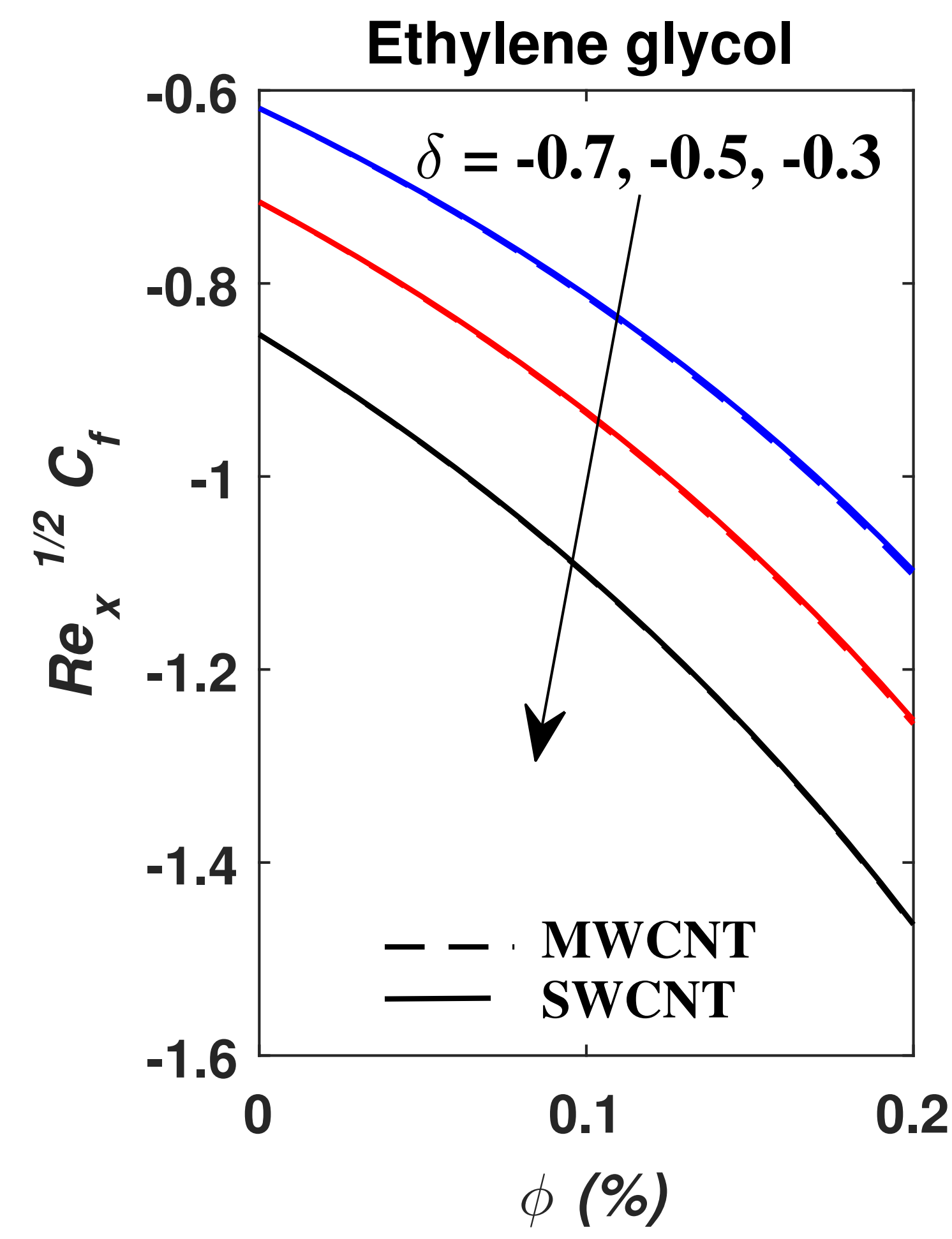
Ethylene glycol
-0.6
-0.8
-1
-1.2
-1.4
-1.6
$Re_x^{1/2} C_f$
δ = -0.7, -0.5, -0.3
MWCNT
SWCNT
0
0.1
0.2
ϕ (%)

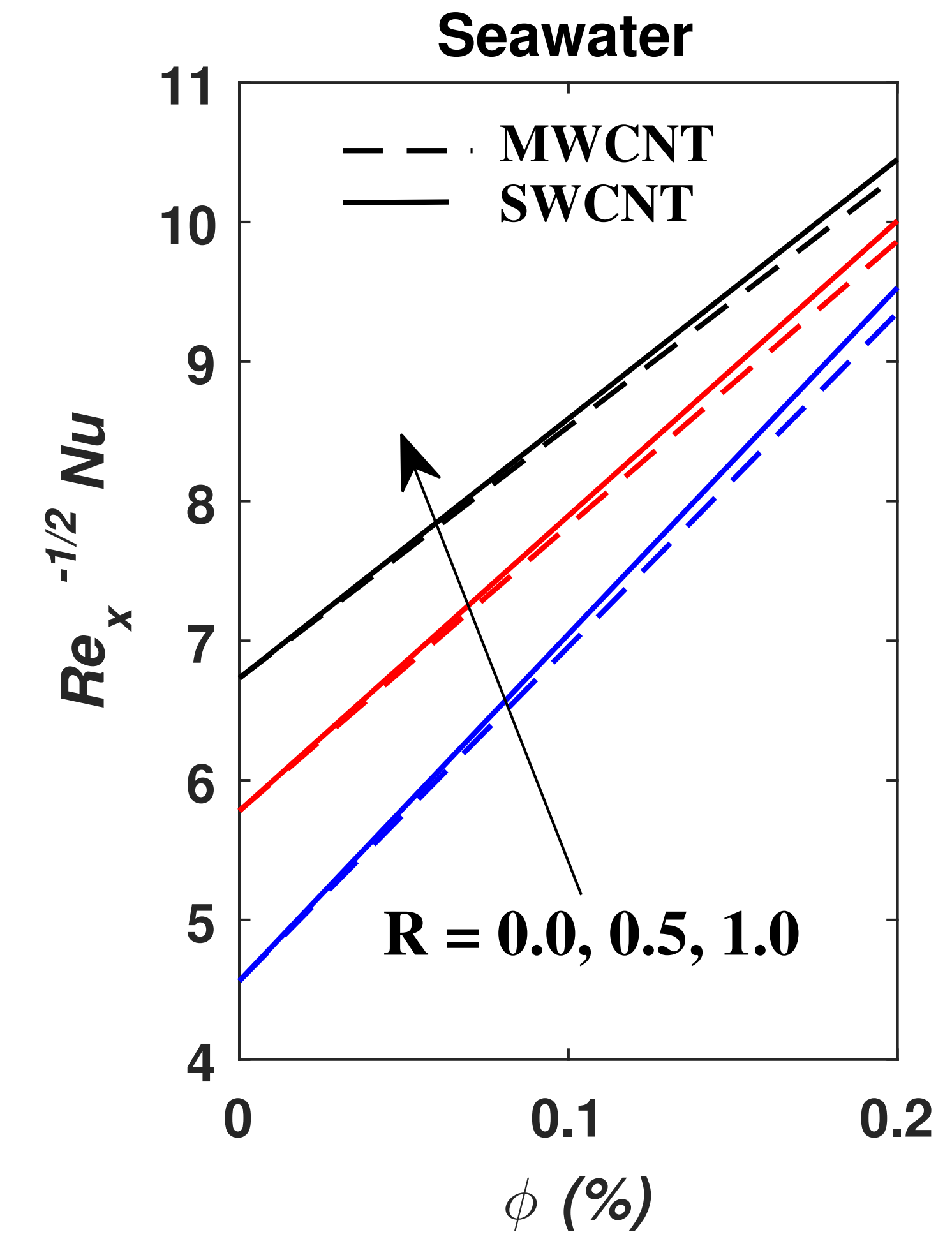
Seawater
MWCNT
SWCNT
R = 0.0, 0.5, 1.0
$Re_x^{-1/2} Nu$
ϕ (%)
11
10
9
8
7
6
5
4
0
0.1
0.2

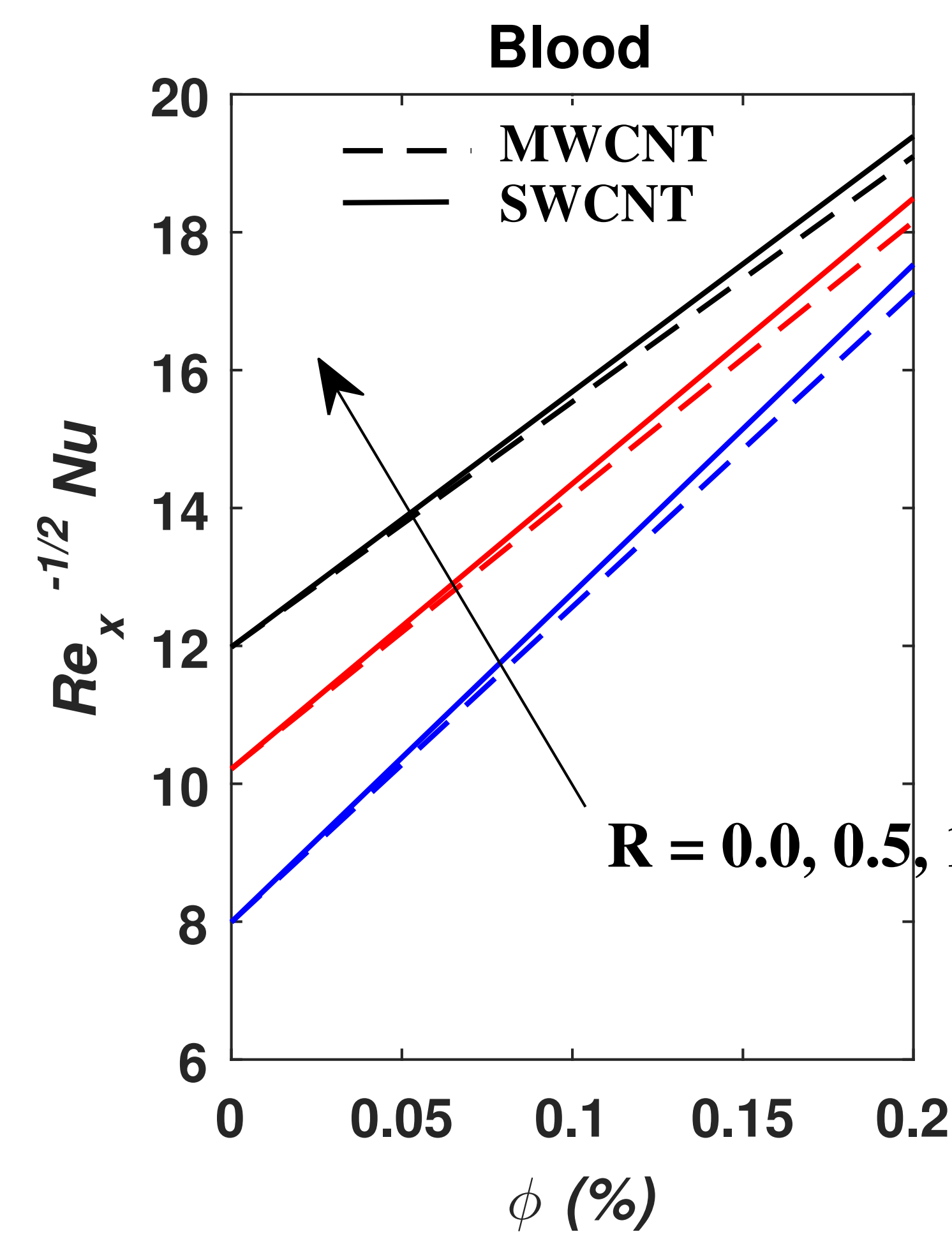
Blood
MWCNT
SWCNT
R = 0.0, 0.5,
$Re_x^{-1/2} Nu$
ϕ (%)
20
18
16
14
12
10
8
6
0
0.05
0.1
0.15
0.2

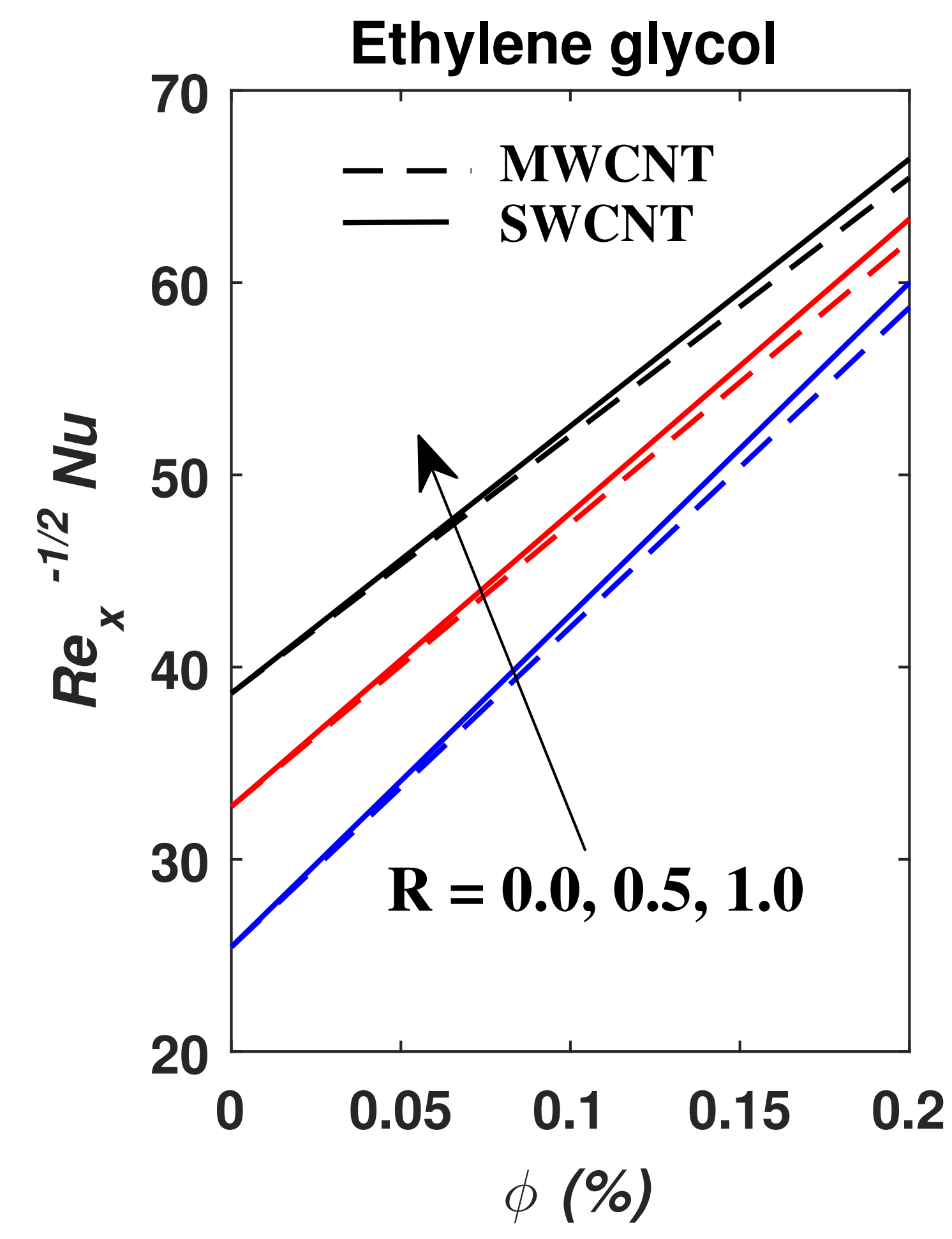
Ethylene glycol
MWCNT
SWCNT
R = 0.0, 0.5, 1.0
$Re_x^{-1/2} Nu$
ϕ (%)
70
60
50
40
30
20
0
0.05
0.1
0.15
0.2

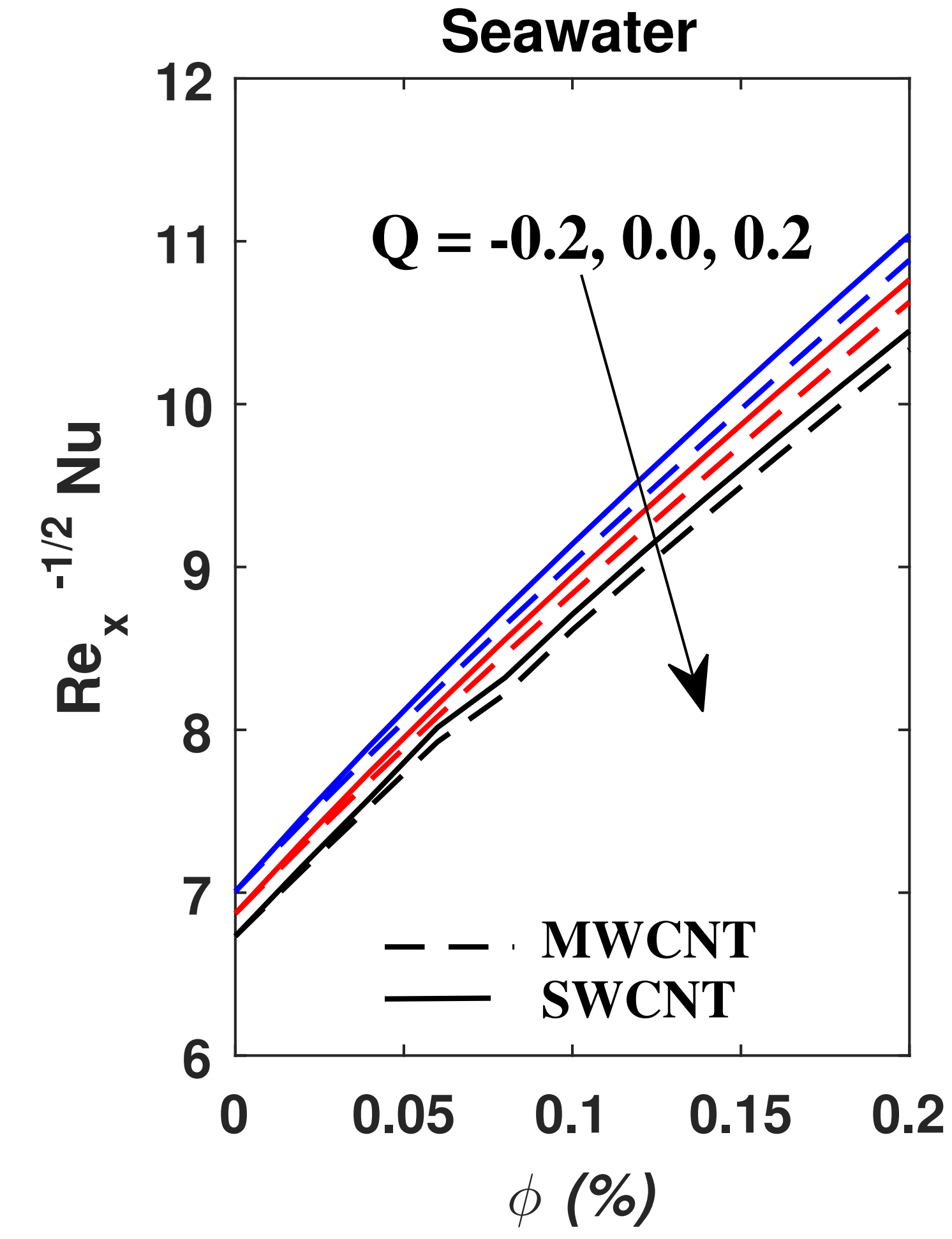
Seawater
Q = -0.2, 0.0, 0.2
MWCNT
SWCNT
$Re_x^{-1/2} Nu$
ϕ (%)
12
11
10
9
8
7
6
0
0.05
0.1
0.15
0.2

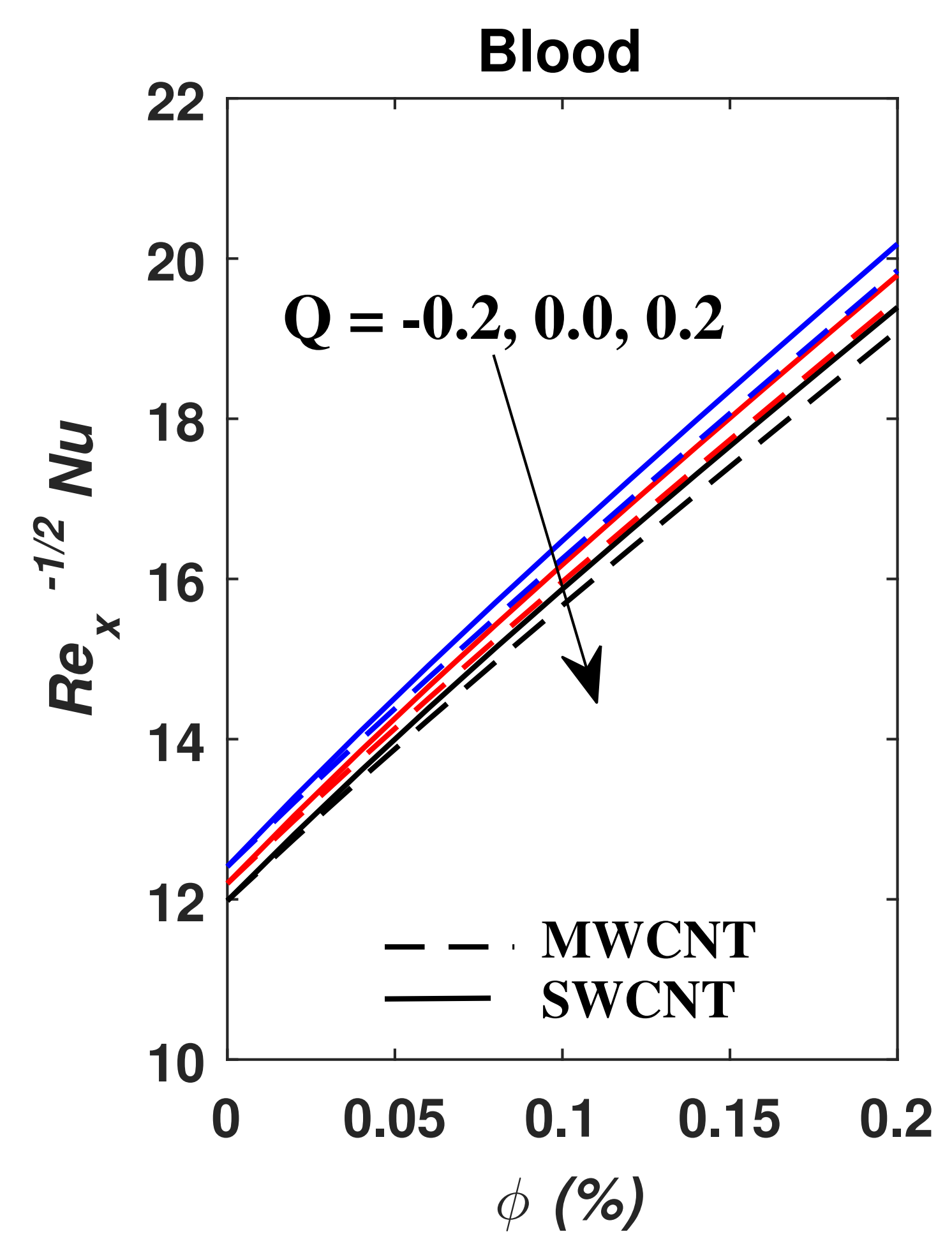
Blood
22
20
18
16
14
12
10
0
0.05
0.1
0.15
0.2
$Re_x^{-1/2} Nu$
ϕ (%)
Q = -0.2, 0.0, 0.2
MWCNT
SWCNT

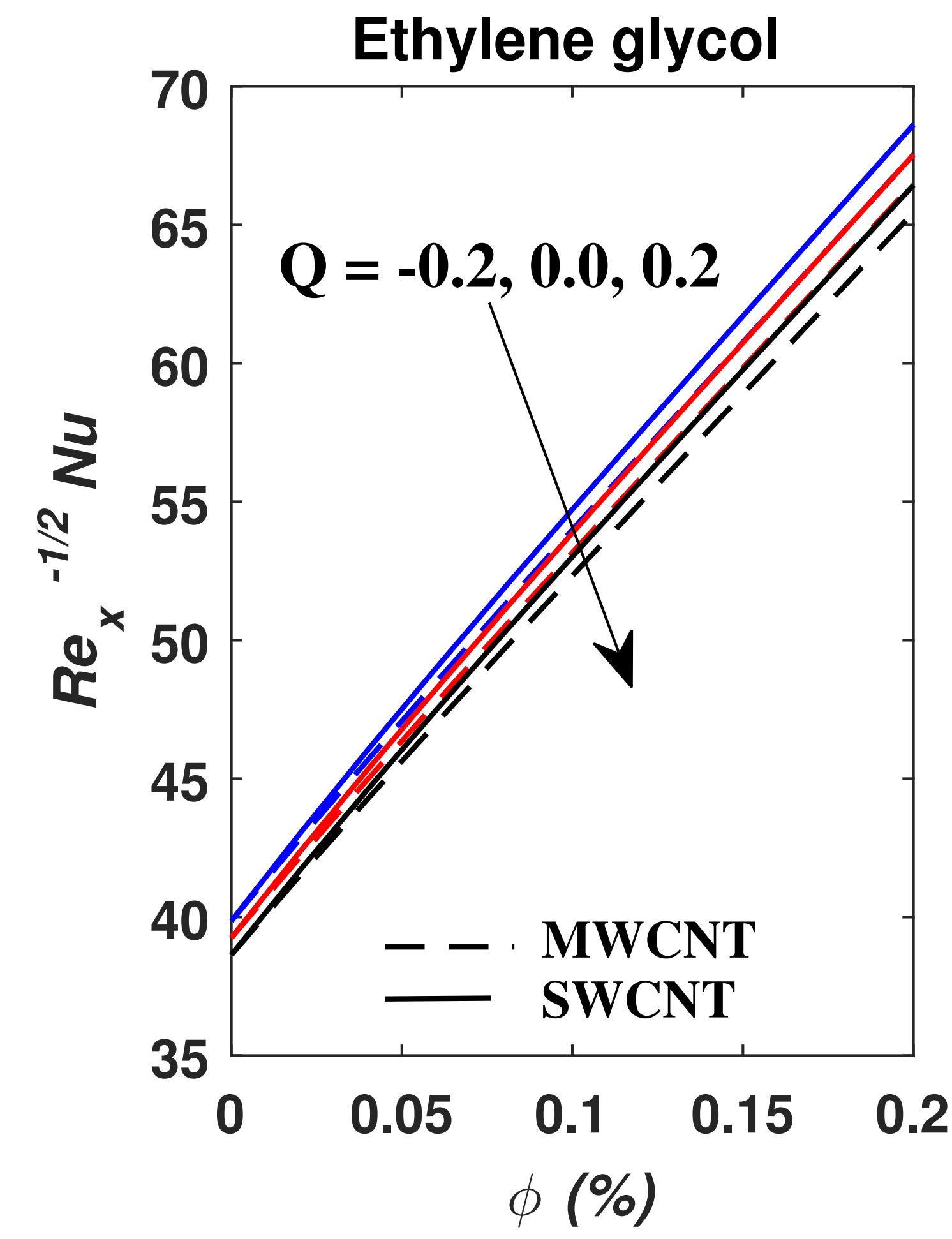
Ethylene glycol
70
65
60
55
50
45
40
35
0
0.05
0.1
0.15
0.2
$Re_x^{-1/2} Nu$
ϕ (%)
Q = -0.2, 0.0, 0.2
MWCNT
SWCNT

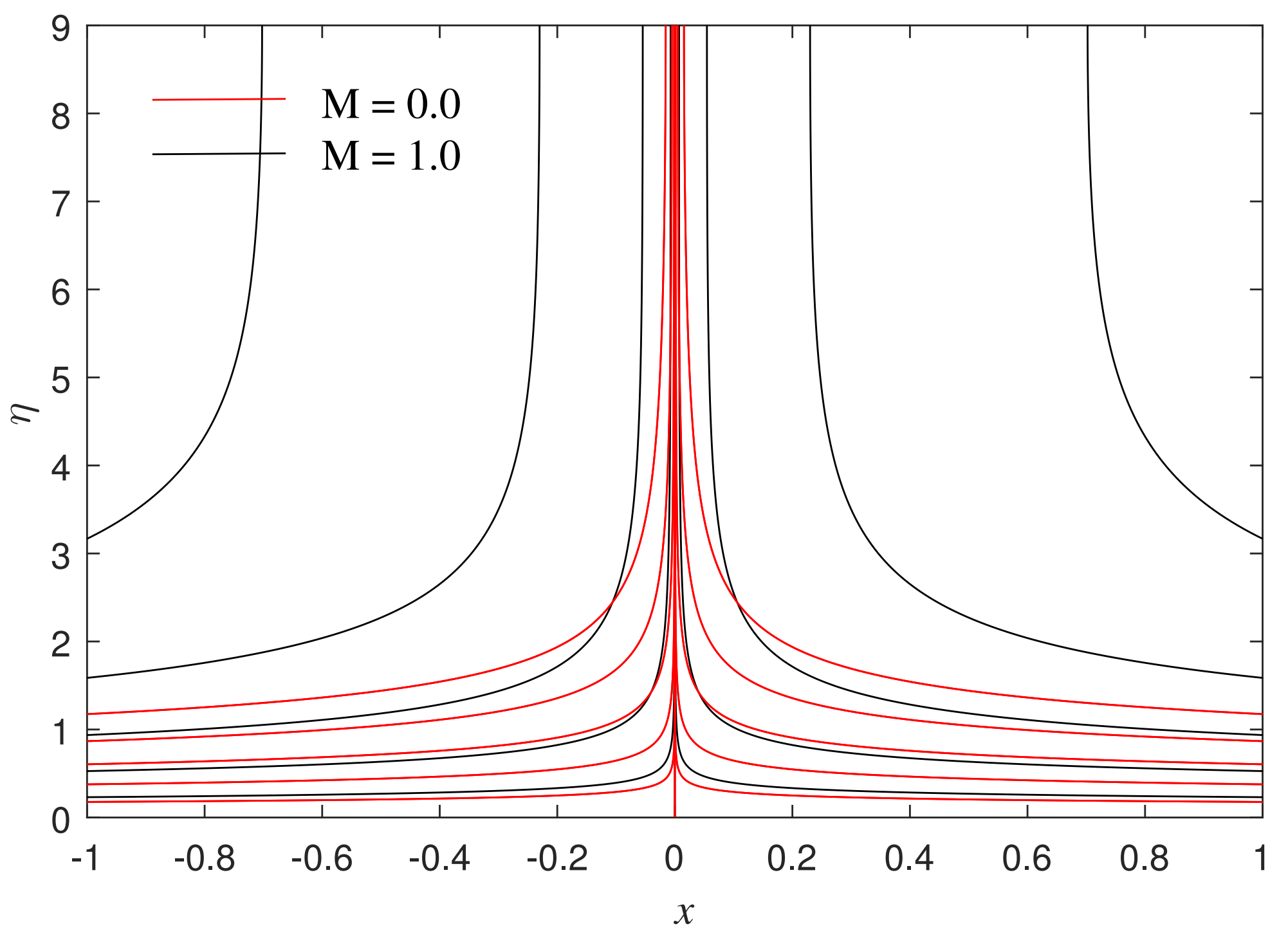
M = 0.0
M = 1.0
9
8
7
6
5
4
3
2
1
0
η
-1
-0.8
-0.6
-0.4
-0.2
0
0.2
0.4
0.6
0.8
1
x

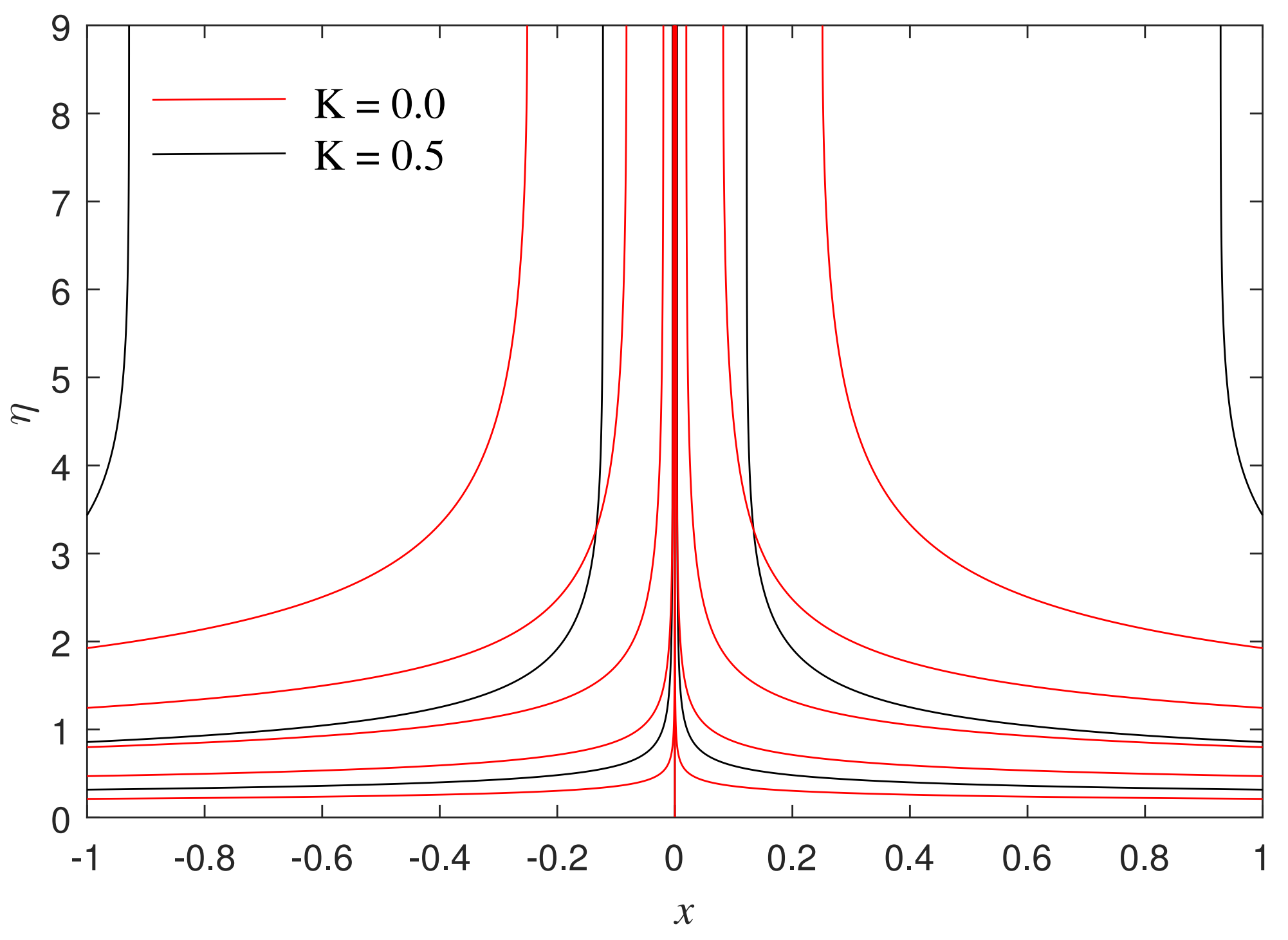
K = 0.0
K = 0.5
9
8
7
6
5
4
3
2
1
0
η
-1
-0.8
-0.6
-0.4
-0.2
0
0.2
0.4
0.6
0.8
1
x

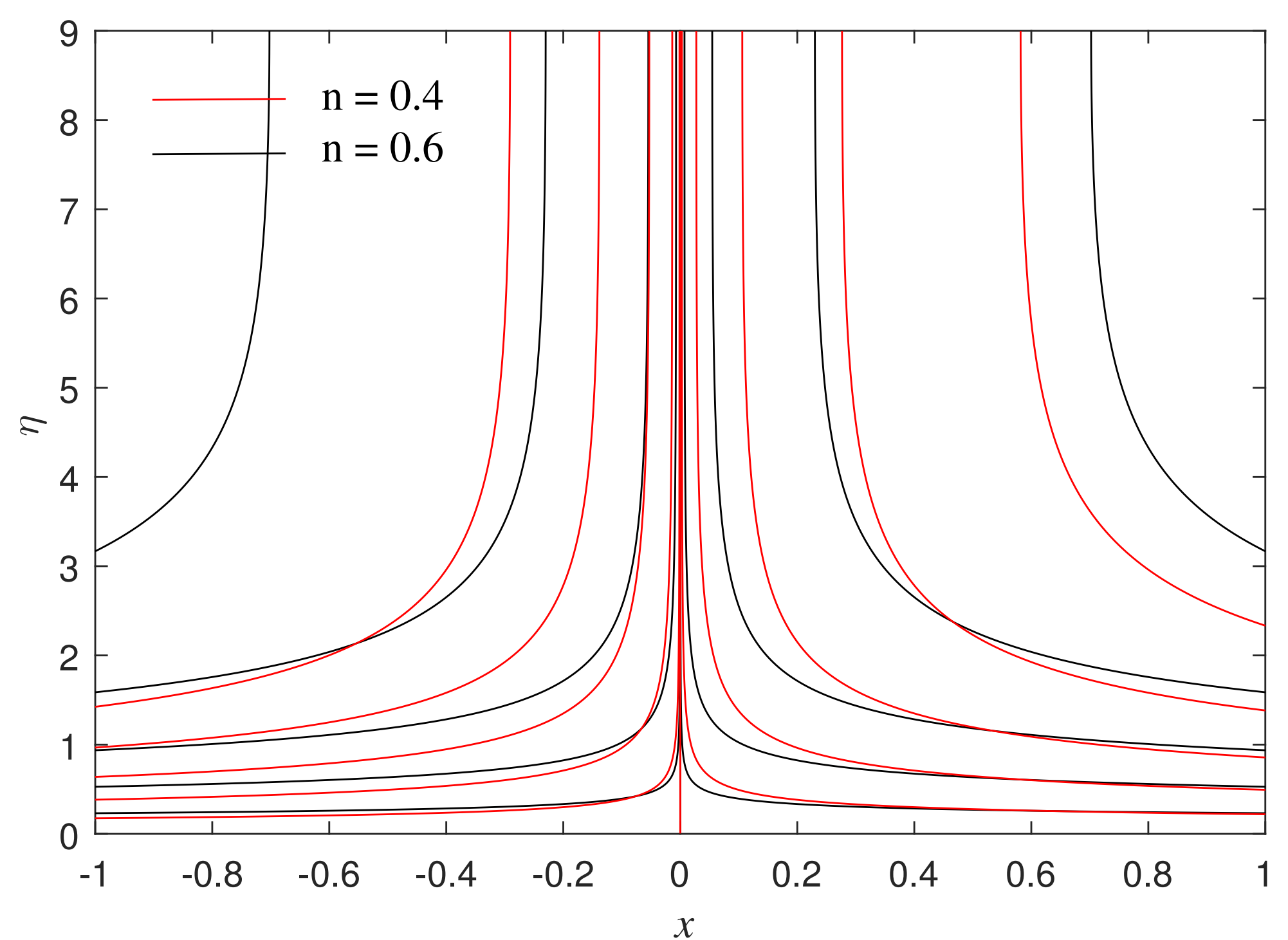
n = 0.4
n = 0.6
9
8
7
6
5
4
3
2
1
0
η
-1
-0.8
-0.6
-0.4
-0.2
0
0.2
0.4
0.6
0.8
1
x